Tribological Investigations of Composites and Other Selected Materials Sliding Against Vacuum-Deposited MoS₂ Coatings

A.W. Ruff
M.B. Peterson

U.S. DEPARTMENT OF COMMERCE
Technology Administration
National Institute of Standards
and Technology
Institute of Materials Science and Engineering
Gaithersburg, MD 20899

NIST

Tribological Investigations of Composites and Other Selected Materials Sliding Against Vacuum-Deposited MoS₂ Coatings

A.W. Ruff
M.B. Peterson

U.S. DEPARTMENT OF COMMERCE
Technology Administration
National Institute of Standards
and Technology
Institute of Materials Science and Engineering
Gaithersburg, MD 20899

ABSTRACT

A new materials approach for rolling element bearings in space
satellite systems involves the use of solid lubricating retainers
and bearing elements vacuum-coated with MoS_2. Improved vacuum
deposition methods are now available to produce dense, suitably
oriented, durable films of molybdenum disulfide. It is of
interest to examine materials in sliding contact with such films
in order to identify suitable combinations, and to further improve
tribological performance of the system. Results of wear and
friction measurements are presented on a number of materials
including self-lubricating composites sliding against four
different types of vacuum-deposited MoS_2 films. The testing
program utilized a controlled environment, pin-on-ring
tribometer, with load and speed conditions appropriate to a
possible application. Differences in wear over 4 orders of
magnitude, and friction up to a factor of 7, were measured among
the materials. Several promising material combinations are
identified.

TABLE OF CONTENTS

A. Introduction

A1. Role of retainer in bearing operation

Rolling element bearings for space applications may be either full complement or partial complement [1,2]. The full complement design places as many balls of the desired size as possible around the circumference of the inner race. Some clearance between any ball pair may be present at rest, but in motion there will be ball-ball contact for every pair for some fraction of the operating time. The partial complement design involves substantially larger clearance between every ball pair. A fourth bearing element, the ball retainer or separator, is added to maintain individual ball position and separation. A schematic of a portion of a partial complement bearing is shown in Fig. 1. In this design, ball rotation on the races implies some sliding contact between every ball and the retainer, somewhere in the "pocket area" for each ball. Clearance in the pocket for each ball depends on the bearing design, and clearance changes with wear of the retainer. Forces at the ball-retainer contacts vary considerably as a function of the applied load (radial or thrust), momentary position, and other aspects of the general dynamic response of the bearing. The retainer rotates at some average angular velocity relative to the races, and it also makes contact with each race either by design or on occasion. Thus while partial complement bearing designs avoid ball-ball contact, they always involve ball-retainer sliding contacts as well as retainer-race sliding contacts.

The details of these retainer contacts during operation depend on the bearing design. Generally, forces on the retainer are not relatively large. External loads only affect the retainer through the dynamic response of the bearing elements, i.e. are not directly applied to the retainer. However, transients in bearing operation caused by external force changes can lead to large momentary forces on retainers as the bearing elements respond to those changes. While retainers usually play a passive role during operation, there is opportunity for an active role such as lubricant re-supply [3,4]. In some liquid lubricated bearings, an oil-impregnated, porous retainer is used. If operation involves any period when oil film deficiency occurs, it may be possible for oil to move from surface pores out toward the ball or race contact, and thus supply an incremental amount of additional oil. A similar active concept could apply to solid lubricated bearings. That concept is shown schematically in Fig. 2 where the composite that contains a solid lubricant phase dispersed within a matrix interacts under load with the lubricating interface film on the counterface. Such self-lubricating composite materials have wide application in a variety of tribological systems (Table 1).

A2. Current retainer materials of choice

Oil-lubricated rolling element bearings for space application currently use either metal or polymer retainer materials. In the case of metals, steel and bronze alloys are customarily used and have well established performance and design guidelines. Steel offers low relative cost and adequate material strength even in relatively thin gauge. Many different retainer geometries are used, mostly in one piece construction. Corrosion can be a problem if

1

humid air environments are involved. Bronze alloy retainers are usually machined. They are copper-tin alloys of various proportions and may contain up to 2 wt. pct. Pb. The hardness, strength, and wear characteristics all depend on alloy composition and processing treatments. Porous bronze is used in some designs with lubricating oil contained within some pores.

A wide variety of polymer materials have been used for retainer construction [5-7]. They include bakelite, PTFE composites, and polyimides, among others. As a class polymer retainers have lower mass than metallic retainers, hence retainer design and dynamics are considerably different. Many commercial polymer retainer materials are composites and contain either or both of (i) solid lubricants, and (ii) hard fibers or particles. Those constituents are added at volume proportions of 10 - 20 % each. The role of those constituents is respectively (i) to contribute to friction reducing films at contact surfaces, and (ii) to provide creep resistance to the bulk polymer, and in addition to remove by abrasion a portion of the surface film that forms. In some cases porous polymer retainers are used, after being impregnated with lubricating oil, to serve as an oil replenishment source for the bearing. Fabrication of polymer retainer elements employs the usual processing methods such as extrusion and casting. Some finish machining methods may be required. While corrosion is not a concern for polymer retainers, there may be significant effects of water vapor on some of the constituents in the composite.

A3. Issues on change from liquid to solid lubricants

Considerably more experience is available on oil lubricated rolling element bearings than on solid lubricated bearings. Nevertheless results so far with both types have identified many of the significant issues that must be resolved. Oil lubricated bearings usually operate in a range of temperature and rotational speed so that an adequate or nearly adequate (boundary lubrication regime) oil film thickness is maintained at the ball-race contacts. This may require a heat source for the oil or the bearing in space applications. A lubricant supply system, e.g. reservoir, pump, distribution lines, must be provided. These requirements lead to additional mass and complexity in the overall system. Special base oils and additive systems have been formulated for space applications, so that storage and testing on the ground and operation in space can both be properly accomplished. Friction forces or torques can be low and steady in such systems, and operating lifetimes in the best cases can be in excess of 100 million revolutions for unidirectional rotation. Figure 3 shows wear rates of a variety of solid lubricant materials from bench tests under different conditions of load and speed. The data are compared to typical wear rates of metallic retainers tested under oil lubricated conditions typical of a rolling element bearing (assuming boundary lubrication). The comparison shows that improvements are needed in solid lubricating materials before they are as effective as oil lubricated retainers. In systems that operate intermittently and bidirectionally, conditions are more severe and lifetimes are reduced.

There are reasons, however, to consider substitution of solid lubricated bearing systems for liquid lubricated bearings. Weight savings and system size reductions can be significant. System complexity would be reduced, and

2

that is always of interest for space systems. However, principal requirements are always performance and reliability, and these must not be compromised. Until recently solid film lubricants had not been extensively used for critical rolling element bearing applications. This was largely the result of the methods used in applying and bonding films such as MoS_2 [8] or graphite [9], and their influence on performance. It was difficult to bond films of uniform thickness, and to avoid loose powder that became loose particulates in the system during operation. Typically binders and adhesive-like carrier materials were necessary additions to the solid lubricant powders. The durability of the applied coating depended largely on its adhesion characteristics, and on the temperature and cohesion characteristics of the binder phase. More recently, vacuum deposition methods have been improved and used to produce dense, adherent solid lubricant and metallic films. Table 2 lists some reported lifetimes for solid lubricated rolling bearing applications. The data points shown in Fig. 3 apply to a number of different solid lubricant materials reported in the literature. Thus one sees evidence of promise for some types of solid lubricating materials in rolling bearing systems.

A4. Requirements on retainer for solid lubricated rolling bearings

Existing design criteria for retainers in oil lubricated rolling bearing systems adequately describe the necessary geometric and mechanical requirements. Debris produced by wear of the retainer is accommodated largely by removal to a filter or sump as oil flows through the system. Any debris that remains on the races will affect the oil film present and is of concern for proper bearing operation. However, in a solid lubricated system, there is no controlled removal process for wear products. Therefore, the retainer must be designed to have a low wear debris production rate, and to produce debris particles that are small in size compared to the solid film thickness and that are compatible with the film itself. Clearances in the retainer must be appropriate to the need to accommodate a changing interfacial film consisting of the debris-solid lubricant mixture. Traction forces on the retainer will depend on the friction present and may change during use. This must be factored into the dynamics of the bearing design.

A5. Inert vs. active retainer material concept

Two concepts for the retainer material role during operation can be considered: inert and active. An inert retainer material is one whose mechanical and chemical influence on bearing operation is negligibly small. Wear debris from such a retainer would not compromise the solid lubricant coating. An active retainer material is one whose influence is to extend the life of the bearing by replenishing the solid lubricant coating. Thus the material must be a composite containing a solid lubricating phase that is released during retainer wear, and that becomes functional when incorporated into the lubricating film in the bearing. The purpose of the NIST project was to develop the knowledge base for inert and active materials and composites for bearing retainers in solid lubricated systems.

3

A6. <u>Film wear model: qualitative</u>

The concept in this project of a dynamic solid lubricating film is shown schematically in Fig. 4. At any time during operation, the film on the counterface {race or ball} is undergoing changes that include wear and loss of material, as well as incorporation of new material that is worn from the composite {retainer}. Debris worn from other bearing elements may also be incorporated. An inert {retainer} material would have different chemical but similar physical behavior to that shown in the sketch.

A7. <u>Critical issues</u>

Solid lubricated rolling element bearings potentially offer simple, self-contained systems of low cost and low maintenance [4,10]. They have high temperature and high vacuum capability. However, there must be a better understanding of wear and transfer processes associated with the ball/retainer and the ball/race contacts. That knowledge base would permit optimization of bearing materials and design for low wear, low steady friction, and long life. There must also be knowledge of traction coefficients in such systems, and the design criteria for bearing clearance calculations.

B. <u>Processing Methods for NIST-prepared Composite Materials</u>

B1. <u>Copper matrix - intercalated graphite materials</u>

One promising system for an active retainer material was a copper matrix - graphite composite [11]. Copper and graphite were known to be compatible materials, and both have had many applications in tribology. Copper can be readily alloyed to alter its mechanical behavior, and it offers good thermal properties. Graphite is a lamellar solid (Fig. 5) that deforms at low stresses by slip between basal planes [9]. It is well established that moisture is needed to facilitate slip, and that its role can be reduced by intercalation of the graphite with inorganic salts [12]. $NiCl_2$ (43 wt. %) - intercalated graphite (IG) was chosen in this study [13]. The IG particles are shown in Fig. 6. The material was reported to be stable up to 325 C, above which decomposition and emission of chlorine fumes occur.

Specimen were fabricated as cylindrical pins, 6.25 mm in diameter, by several methods. Powder-compacted pins were made in a hydraulic press using a steel die at forces of 22 to 44 kN (pressures of 0.7 to 1.4 GPa). Pure pins of copper and of IG were made separately by powder compaction. Compacts of pre-mixed powder combinations of copper and IG were also made. Figure 7 shows examples of the microstructure of two mixed compacts. We found, typically, good bonding between most of the copper particles, and a reasonably uniform distribution of the IG phase. Some surface cavities can be noted in the IG phase regions which may be voids resulting from compaction, or may have resulted from the preparation of the polished surface. Thermal sintering treatments were not used on the materials discussed here.

Two types of manufactured composites were also used. One contained a series of holes in an hexagonal arrangement with different hole diameters and

separations, and the other contained a central slit with different widths. IG powder or mixtures of Cu and IG powder were compressed into the holes or slits using the same hydraulic press and die system and the same range of pressures. Both specimen types are shown in Fig. 8 using specimens photographed after use in one test. The hole and slit size variations permitted different effective area and volume percentages of IG and copper under controlled phase shape and spacing. All composite specimens were stored in desiccated chambers after fabrication to minimize effects of water vapor prior to testing. Hardness measurements were carried out on some of the composites using the Rockwell superficial method, scale 15T. Those results are shown in Fig. 9.

B2. Bronze matrix - molybdenum disulfide materials

It was not possible to obtain satisfactory powder compacts of bronze and MoS_2. The compacts that were made did not have sufficient mechanical strength. This may have resulted from the formation of an MoS_2 film on the surfaces of the bronze particles that prevented adequate adhesion during pressing. Another method was developed for preparing bronze composite specimens. The method involved infiltration of a porous bronze matrix with a suspension of submicrometer sized MoS_2 particles [14] in ethanol, followed by evaporation of the ethanol. Good results were obtained using a 20 μm pore size, a bronze density of about 50 %, and several cycles of infiltration to a final content of 10 vol. % MoS_2. Mechanical compression of the specimens in a steel die then followed to increase final density. Further details on preparation of these specimens are shown in Table 3. Composites containing up to at least 20 vol. % MoS_2 could be prepared in this way. Typical microstructure of the composites is shown in Fig. 10 where the medium grey toned regions are the MoS_2 phase, and the black regions are voids that remained.

C. Results for Composites Sliding on 440C Steel

C1. Sliding test method for uncoated rings

Wear tests were carried out using two configurations of a sliding pin-on-ring tribological test system. One configuration permitted loading two pins simultaneously against a rotating steel ring; the other utilized a holder carrying a single pin. The rings were type 440C stainless steel, tapered bearing cups, 35 mm diameter, 8 mm wide, having a hardness of HRC 58 and a surface finish of 0.15 μm RMS. This material was chosen in view of its wide application in advanced rolling element bearing systems. Tests were carried out in either laboratory air or dry argon at normal ambient temperature, in order to determine sensitivity to water vapor and oxygen. A small chamber into which argon gas was continually fed surrounded the specimens during those tests. The relative humidity in the lab air tests ranged from 10 to 40 percent. For all tests reported here, the load was 33 N, the sliding speed was 0.14 m/s, and the sliding distance was 790 m. Figure 11 shows a photograph of the tester with the sample environmental enclosure mounted in place. The lower photograph shows the specimen holder with a test pin in place, and a test ring lying adjacent.

C2. <u>Wear mechanism for composites</u>

Figure 12 shows an SEM image of a portion of a wear scar near four IG regions in a manufactured Cu-IG composite pin. A similar area on another specimen is shown in more detail in Fig. 13. It was found that in both the particulate and the manufactured composite specimen cases, an interfacial film was established in the contact zone. In Fig. 12 the film lies to the left side of one IG region, specifically the exit side relative to the sliding direction. Loose wear debris particles were also found remaining in the contact gap. A third significant observation concerned surface recession at the soft IG regions, typically by 1-5 μm. Each of these characteristic features, shown in the sketch in Fig. 13, is thought to be important in the wear and friction mechanisms involved in the tribology of self-lubricating composites, and will be discussed later.

The interfacial films formed during sliding were found on both the test pins and on the steel rings (Fig. 14). While patchy in distribution and non-uniform in thickness, it was clear that the films were a principal factor controlling wear and friction behavior. Films were characterized on several specimens, dimensionally and compositionally. Figure 15 shows the surface topography of a portion of one Cu-IG interfacial film measured by stylus profilometry across the wear track on one of the test rings. In this case the average film thickness was 1.1 μm, relative to the ring surface outside the wear track. Some film patches were as thick as 10 μm. Observations involving the bronze - MoS_2 composite specimens and matching test rings were basically the same as described above.

C3. <u>Interface film morphology</u>

The composition of the interfacial films was also important. The film was found to contain all of the system wear products, for example, IG, copper, steel, and possibly oxides, based on x-ray microanalysis of the films . Figure 16 shows X-ray spectra from three different film regions involved in a Cu-IG test. In Fig. 16a, the film region is on the composite pin, from a region overlaying the copper matrix, immediately at the exit side of an IG phase region. In Fig. 16b, the film region is on the composite pin, well removed from any IG phase region. Finally, in Fig. 16c, the film region is from the steel ring surface. In the spectra, the Cu peak originates from wear products in the film, as do the Fe, Cr, and Ni peaks. The Cl peak can be used to determine the amount of IG present, sinced CI comes from the $NiCl_2$ intercalant. For thicker regions of the film, such as in Fig. 16a, we find proportionally greater amounts of IG (denoted by the Cl peak), and of pin wear debris (denoted by the Cu peak). For thinner regions of the film, such as in Fig. 16b, we find proportionally less IG and higher Fe and Cr peaks from some steel ring wear products.

C4. <u>Air vs. dry argon effects during sliding</u>

It was readily apparent early in the test program that significant effects could be associated with the test atmosphere. The laboratory air atmosphere contained substantial amounts of water vapor (relative humidity ranged from 15 to 40 %) and oxygen, while the controlled, dry argon atmosphere contained

neither of those species. As shown in Fig. 17, interruption of the dry argon gas allowed lab air to infiltrate into the test atmosphere, and this change caused a significant increase in system friction. The effect was always repeatable. In view of this sensitivity, separate tests were carried out in the two atmospheres.

C5. Wear and friction results

Pin wear volumes were calculated from pin wear scar dimensions. Wear on the rotating ring counterface was not appreciable in any test, although there was some small contribution to the wear debris produced, determined by the presence of Fe lines in x-ray microanalysis spectra from the surface films present. Pin wear accounted for virtually all the system wear under the present conditions.

Friction and wear results from the Cu-IG composites obtained in laboratory air are shown in Fig. 18. From 3 to 5 individual tests were conducted for each of the values of volume percent IG. The average values and a range of ± one standard deviation are given. In the figure the dashed line shows the measured values for 2-pin tests of copper and IG. These results are taken as baselines for friction and wear since the separate IG pin in a two pin test can supply as much material as needed according to its wear rate. For the composites it is seen that friction coefficient decreases from a value of about 0.5 for copper to values about 0.15 as the IG fraction increases. Most of the decrease occurs by about 30 vol. % IG. The wear rate results (Fig. 18b) show a significant reduction on adding up to about 10 vol. % IG. Higher amounts of IG than this led to increased wear. This type of behavior suggests that two separate processes are involved. It is thought that since higher amounts of IG are associated with lower copper fraction in the composite, mechanical weakening in the supporting copper matrix takes place at higher levels of IG content, and this leads to the observed wear increase. When the wear data were normalized by the volume percent Cu in each composite, the influence on the wear data of the matrix strength is removed, and a monotonic decrease in normalized wear with increasing IG fraction was found. This is equivalent to applying a rule-of-mixtures for the influence of composite strength on wear. Most of the beneficial effect on wear is accomplished by adding up to 15 vol. % IG.

Results for friction and wear of the composites in a dry argon atmosphere are shown in Fig. 19. Only average values are shown for clarity, but each average involved 3-5 separate tests and the typical scatter is similar to that shown in Fig. 18. While the general trend is similar to the laboratory air test results, there are significant differences for the lower IG concentrations. For composites with less than 10 vol. % IG, the sliding friction coefficient was about 25 percent lower in argon. Even larger effects were found in wear rate in argon, where a reduction by a factor of about 3 is seen for composites with less than 25 vol. % IG. Above 30 vol. % IG there was no significant difference in wear between the two atmospheres.

The causes for these reductions in friction and wear are believed to involve two effects. First, the interfacial film in the contact probably changes in the presence of sufficient water vapor and oxygen through chemical interaction

7

of the IG. It was observed early in this work that water vapor was slowly adsorbed by any composite specimens left exposed to lab air for a significant length of time; this was possibly due to hygroscopic action of excess $NiCl_2$ left in the IG during manufacturing. Similar sensitivity to water vapor would be expected on the part of the steady-state interfacial film in the sliding contact region. Film adherence, thickness, and area coverage would likely all be affected. Visual observations on the steel test rings showed smoother, more uniform interfacial films on argon-tested specimens compared to air testing. It is thought that smooth, uniform films lead to improved friction and wear properties.

A second effect might involve the oxide films present on the copper and steel test surfaces. Changes in availability of oxygen and water vapor from the atmosphere during sliding would be expected to affect oxide film thickness and formation rate. From x-ray surface microanalysis results it is clear that the interfacial film is a complex mixture of wear products from the metal surfaces and the IG. Changes in relative proportion of these film constituents would be expected to affect film properties, e.g. cohesion and adhesion. In fact for the case of no IG additions, we also see an effect of test atmosphere on wear, involving only metal and metal oxide debris in the film. Further quantitative study of film composition and its effect on film properties would be desirable to understand these findings.

Microstructure effects on wear of the composites were also found. One manufactured composite pin specimen was made with small, close-spaced holes containing IG at an effective amount of 42 vol. %. As shown in Fig. 18, that specimen had significantly lower wear compared to that found for the two adjacent powder compacted specimens. Examination of wear surfaces after several tests of that specimen showed a greater coverage of the copper matrix area (on the pin) by the interfacial film created near the exit side of each IG region. This suggests that lower values for matrix mean-free path may be desirable in the composites to allow for film development over as much of the matrix region as possible. A second issue concerns desirable size for the IG regions. One important feature of the IG regions in these composites was recession of the surface, shown schematically in Fig. 13. Typical recession amounts were 1-5 μm. The recession is due to preferential wear of the soft IG region by wear debris in the contact. Some of the debris particles also collect near the entrance edge of the region (Fig. 13). It is thought debris collection could effectively block the region from providing additional IG to maintain the interfacial film in the contact, and that this process may determine a lower size limit for the IG regions. If the size is too small, the provision of fresh IG from the region would cease. The mean size of the IG regions in the powder compact composites was about 20 μm, and apparently was sufficient to preclude such debris blocking.

Wear and friction results for the bronze - MoS_2 composites were similar in overall features to those for the Cu-IG materials. They are shown in Fig. 20 for the tests in dry argon. Both friction and wear rate decreased by about a factor of 4 upon adding 20 vol. % MoS_2 to the bronze. At higher concentrations the values remained the same or increased slightly. Clearly an effective concentration of MoS_2 in bronze was in the range 10-20 vol. %.

C6. Film wear model: quantitative

A simplified analysis of wear in self-lubricating composites is presented next, following the model shown schematically in Fig. 4. Consider that at steady state the thickness of the IG interfacial film is affected by (1) growth as IG worn away from the composite is added to the film, and (2) loss as the film itself is worn away. An inequality relating wear volume per unit sliding distance per unit contact pressure, W', for the film (f) and the lubricant phase (lp) in the composite as follows:

$$W'_{lp} > W'_f. \tag{1}$$

This can be expressed using the Archard-Holm wear equation as:

$$K_{lp} A_{lp} / H_{lp} > K_f A_f / H_f \tag{2}$$

where K is the wear coefficient, H the indentation hardness, and A the nominal contact area of the lubricant phase and the interfacial film.

But $\qquad A_f = A_{contact}$

since the film nominally covers the entire contact, and

$$H_{lp} = H_c(\text{composite}); \qquad K_{lp} = K_c(\text{composite})$$

since the lubricant phase is part of the composite, as far as the load distribution in the contact region and wear are concerned.
By substituting these relations in (2) we obtain

$$K_c A_{lp} / H_c > K_f A_{contact} / H_f \tag{3}$$

Thus for the interfacial film to maintain a steady-state thickness, the wear coefficient of the composite is given by:

$$K_c > K_f (H_c / H_f) (\text{lubricant fraction in composite})^{-1}. \tag{4}$$

The observed wear rate (and wear coefficient) for the composites decreases with increasing IG content as seen in Fig. 18. Re-plotting the wear data, normalized by the volume percent Cu to account for matrix weakening, vs. reciprocal volume fraction of Cu allows a comparison with Eqn. 4. This comparison is shown in Fig. 21, where the solid line corresponds to Eqn. 4. All of the composite wear data are consistent with the model prediction, and actually are in excess of that needed to maintain a constant interfacial film thickness. Thus it should be possible to reduce the wear rates of such composites and still provide sufficient new solid lubricant to maintain film thickness. It would also be important to further refine the model to include composite microstructural parameters such as phase diameter and mean-free-path.

D. Fundamental Studies of Interfacial Film Formation

Results obtained during the studies described above on the composites established the importance of the interfacial film in determining system friction and wear. It was felt that additional basic studies were needed to clarify some aspects of the film formation and degradation processes. The 2-pin tests that were conducted in the composite studies revealed information on some of those processes. Figure 22 shows an example of the friction behavior of the sliding system while the interfacial film is forming in the bronze - MoS_2 studies. In this case, the steel ring is initially clean but a film forms quickly in the first cycle of sliding to produce a friction coefficient of about 0.18. Afterward, up to a total sliding distance of 800 m, the friction coefficient decreases slowly to 0.1. Thus it is seen that the final film formation process is gradual. Throughout the process, however, there are significant excursions to higher friction values. Even at a distance of 740 m, an excursion can be seen to a friction value of 0.21. These brief, high values probably indicate processes of film destruction, locally, and they are followed shortly by film repair processes.

In order to gain more information on the interfacial film, a pin-on-disk tribometer was developed that would allow interruption of sliding for the purpose of film examination and measurement. The system is shown schematically in Fig. 23. It consisted of a rotating steel disk and a stationary pin that could be either a solid lubricating material or a composite. A stylus profiling head was placed so that the wear track (transfer film) formed on the disk by the pin could be traced in the radial direction. A 1.2 mm diameter steel sphere was used for tracing the relatively soft films at a light load of about 10 mN. The tribometer would operate by rotating one or several cycles with a load on the pin, then stop at an indexed position so that the profile of the wear track could be obtained. Additional rotation cycles would then be done, followed by another profile trace at the same location.

It was possible to calculate the average thickness of the pin wear track from the individual profiles, and one such result is shown in Fig. 24. It shows the track thickness increasing gradually up to 0.1 μm after 300 cycles at a load of 1.7 N using an MoS_2 pin and a 52100 steel disk. There are large variations in average film thickness from one cycle to the next. The individual profiles can also be combined into a time-based or revolution-based representation of the track topography. One example is shown in Fig. 25. There the first 300 cycles of sliding formation of an MoS_2 film is shown, traced across the wear track. Note the appearance and disappearance of several features in the film topography as its thickness gradually increases. From these studies of film formation it was clear that thicknesses at steady state were in the range 0.5 to 10 μm, and that the films were quite non-uniform in topography. It was apparent that the addition of wear debris products such as metal oxides or polymer particles would significantly influence film properties.

E. Results for Sliding on MoS2 Pre-coated 440C Steel

A series of sliding tests were conducted on MoS_2 pre-coated steel rings. The

coated rings represented an element in an MoS_2 pre-coated rolling bearing, and the test pins represented possible retainer materials. The MoS_2 coating methods involved vacuum deposition by 4 different approaches, all leading to uniform, high density, adherent coatings [15-18].

E1. Coatings and pin materials studied

A list of the pin materials examined is given in Table 4. Several commercially available materials were included to provide a connection between this study and reported usage in bearing systems. Gold was also of interest as a possible inert material in terms of its potential for wear debris chemical interaction with the MoS_2 coatings. In addition, a Au-Ni electroplated coating was prepared (Table 5) on steel pin substrates for study. That alloy, containing 0.2 wt. % Ni, exhibited a much higher hardness value than the pure gold, yet only had a small amount of additive to the gold, and could be considered essentially inert. Two types of research composites prepared at NIST were included; a copper - $NiCl_2$ intercalated graphite (IG) composite, and a bronze - MoS_2 composite. In both cases the matrix material and the composite were tested separately. The particular compositions chosen, based on the earlier studies described above, were Cu - 20 vol. % IG, and bronze - 10 vol. % MoS_2. The composite specimens were stored in desiccated chambers after fabrication to minimize effects of water vapor prior to testing.

MoS_2 coatings were prepared by several vacuum deposition techniques at other laboratories. The DC sputtering [19], RF sputtering [20], magnetron sputtering [21], and multilayer metal-MoS_2 sputtering [22] methods used have been described previously. These four types (Table 6) will be referred to in this paper as DCS, RFS, MGS, and MLS types, respectively. In all cases the coatings were relatively dense, adherent, and ranged in thickness from about 1 to 5 μm. Previous publications should be consulted for preparation details [19-22]. An example of the morphology of the as-deposited coatings is shown in Fig. 26, an SEM micrograph of a type MGS coating. The linear features in the photograph result from surface scratches on the steel substrate prior to coating.

E2. Test method for pre-coated rings

Sliding wear tests were carried out using the pin-on-ring test system described earlier. The rotating rings were type 440C stainless steel, tapered bearing cups, 35 mm diameter, 8 mm wide, having a hardness of HRC 58 and a surface finish of 0.15 μm RMS. They were coated with vacuum deposited MoS_2 coatings of several types mentioned above. Most of the test pins were 6.25 mm in diameter and from 5 to 10 mm long. The Au and Au-Ni pins were smaller, 3.1 mm in diameter. Two of the polymer materials were obtained in sheet form, and small rectangular blocks, about 2 x 5 x 5 mm, were machined and used. In all cases a rounded end, 6.25 mm diameter, was machined on the pin end used for testing. Tests were carried out in either laboratory air or dry pure argon at normal ambient temperature, usually 25 C. A small chamber into which argon gas was continually fed surrounded the specimens during those tests. The relative humidity in the lab air tests ranged from 15 to 40 percent. For all tests reported here, the load was 33 N, the sliding speed was 0.14 m/s, and

11

the total sliding distance was 1900 m. Nominal contact pressure at the start of a test was about 1.7 GPa, but as the contact wore and the apparent contact area increased, the pressure would decrease to typically 150 - 300 MPa by the end of the test.

E3. Coated ring surface wear morphology

Sliding tests carried out both in lab air and dry argon showed considerable differences among the coatings and in the two atmospheres. Figure 27 is an SEM micrograph from a 1900 m test in lab air using a Cu - 20 vol. % IG pin on a RFS type coating. A wide wear track on the MoS_2 coating is seen in the upper photograph. At higher magnification (lower photograph) one sees a marked change in the coating topography with many small debris particles and lips of material protruding. In contrast, for a similar test in a dry argon atmosphere, Fig. 28 shows a much narrower wear track in the MoS_2 coating and much less disturbance to the coating. Figure 29 shows an optical micrograph of a similar wear track, formed in air using a Au pin on a type MGS MoS_2 coating. Evidence of plowing damage to the coating, and of wear debris particles in the wear track can again be seen. The traced profile of the wear track also shown was taken using a 1.2 mm diameter spherical tip and a low contact pressure. It indicates the amount of material, up to 3 μm depth, lost by wear from the coating whose initial thickness was about 5 μm. Another important consideration in understanding the wear behavior of these deposited MoS_2 coatings concerns composition changes in the coating that take place during sliding. Since measurable pin wear occurred in all cases, wear debris particles became incorporated into the coatings. Examples of this effect are shown in Fig. 30 for the case of Cu-IG sliding on a type RFS coating. Substantial amounts of Cu, Fe, and Cr are seen in the upper EDX spectrum taken from a track worn in air. Much less debris contamination occurs for tracks worn in dry argon (lower EDX spectrum). No such species were found in the unworn coating. It appears that a major factor in determining MoS_2 coating endurance is the effect on coating properties such as shear, cohesion, and adhesion, of any incorporated wear debris or coating degradation products.

E4. Friction results

A wide range of friction vs. time behavior was observed in these tests. The most striking effect was the difference between lab air and dry argon as a test environment. Figure 31 shows a comparison between those two cases for a set of several pin material and MoS_2 coating combinations. In general, friction was higher and more variable in air than in argon. Figures 32 and 33 show more detailed comparisons of friction coefficient vs. sliding distance for 5 materials on one MoS_2 coating in the two environments. Nickel and molybdenum, and to a lesser extent copper, show erratic friction behavior in air, while only nickel shows that type of response in argon. Gold, which forms no oxides to interfere with the MoS_2 coating, shows low, steady friction in both environments. In argon, several materials show steady friction for this particular coating. Ideally one would seek a material combination that led to low, steady friction, such as is shown in Fig. 34a, for the Au-Ni alloy with an MGS type MoS_2 coating. In that case the friction coefficient of 0.05 remains nearly constant for 1900 m of sliding. A different material, the

bronze - 10 vol. % MoS_2 composite gave a somewhat higher friction result (Fig. 34b) on the same coating and was somewhat variable for the first 600 m, but the combination otherwise performed well. Figure 35 contrasts the same composite on two coatings: the MGS type coating in (a) and the MLS type coating in (b). The friction result differs by about a factor of 2, but is reasonably steady in both cases at the end of the test. Figure 36 contrasts the friction results for Au and the Au-Ni material sliding on the same coating, the MLS type, and again both combinations performed reasonably well. Two other examples are shown in Fig. 37 for two polymer composite materials sliding on an RFS type coating in (a) and a DCS type coating in (b). In both cases friction was high initially but then decreased to a lower, steady value, somewhat larger than those for the metal sliders. It is clear that the friction behavior is sensitive to the material combination and the test atmosphere.

E5. Wear results

A comparison of average friction and wear rate values for all the combinations studied in dry argon atmospheres is shown in Fig. 38. Different plotting symbols are used for the four types of MoS_2 coatings. It was found that wear of the pin material varied by over a factor of 20,000 and that friction varied by over 7 times. Several combinations provided values for friction < 0.08 and wear rates < 10^{-6} mm^3/m; such combinations could be suitable for applications. Promising materials were the Au-Ni electrodeposited alloy, bronze, and the bronze-MoS_2 composite. Generally the type MGS coating showed good performance in this test, although endurance life testing would also be needed on the combinations. The polymer materials overall showed significantly higher wear and friction for all coating types studied. An empirical fit to the boundary of the results is also shown in Fig. 38. It emphasizes the strong dependence, to the power 4.6, of pin wear on system friction. This is probably best understood to reflect the importance of traction stresses on such characteristics as local coating thickness (a dynamically changing quantity), local coating durability during sliding, and the effect of incorporation of wear debris and coating degradation products into the MoS_2 coating. In all cases where test were conducted in moist air, wear rates and friction coefficients were found to be significantly higher. The role of moisture and oxygen in degrading tribological properties of MoS_2 coatings is not fully understood but previous findings have also shown that MoO_x and other oxides in the coatings can change performance [23-26].

F. Conclusions

1. The choice of retainer material may have a major effect on the performance of solid lubricated rolling bearings.

2. Composite materials should offer an acceptable option for retainer applications in solid lubricated rolling bearings if properly formulated for the system.

3. Inert retainer materials of the proper type should offer an acceptable option for retainer applications in solid lubricated rolling bearings.

4. Both $NiCl_2$-intercalated graphite and MoS_2 are tribologically effective when added to copper- or bronze-matrix composites.

5. Environment effects on wear and friction of materials sliding against intercalated graphite and MoS_2 films and coatings can be significant.

6. Wear rates of Cu-IG and bronze-MoS_2 composites, sliding against 440C steel, can be 1/5 to 1/10 the values for the matrix alone, and friction coefficients can be as low as 0.1.

7. For the composites studied in sliding against 440C steel, when balancing the tribological and mechanical properties, the optimum volume fraction of the solid lubricating phase was 0.1 to 0.2.

8. An essential element for effective tribological composites is the development and maintenance of a suitable interfacial film at the contact.

9. Wear rates of certain composites, sliding against pre-deposited MoS_2 coatings, can be sufficiently low for consideration as retainer materials in dry argon atmospheres.

10. Friction coefficients of certain composites, sliding against pre-deposited MoS_2 coatings, can be as low as 0.04 in dry argon atmospheres.

11. A suitable metal-matrix composite material for use in sliding against pre-deposited MoS_2 coatings on 440C steel is bronze-10 vol.% MoS_2.

12. A suitable inert material for use in sliding against pre-deposited MoS_2 coatings on 440C steel is a Au-0.2 wt.% Ni electrodeposited alloy.

References

1. L.B. Sibley, "Rolling Bearings" in <u>Wear Control Handbook</u>, ed. M.B. Peterson and W.O. Winer, ASME, NY, 699-726 (1980).

2. T.A. Harris, <u>Rolling Bearing Analysis</u>, J. Wiley, NY (1984)

3. D. Scott and J. Blackwell, "Sacraficial Cage Materials for the in-situ Lubrication of Rolling Bearings," European Space Tribology Symposium, Frascati, April 1975.

4. J.K. Lancaster and P. Moorhouse, "Etched-pocket Dry Bearing Materials," Tribology International <u>18</u>, 139-148 (1985).

5. J.C. Anderson, "Wear of Commercially Available Plastic Materials," Tribology International (Oct. 1982) pp. 255-263.

6. R.L. Fusaro, "Evaluation of Several Polymer Materials for Use as Solid Lubricants in Space", STLE Transactions <u>31</u>, 172-181 (1987).

7. V. Buck, "Self-lubricating Polymer Cages for Space-profed Bearings: Performance and Roundness"

8. W.O. Winer, "Molybdenum Disulfide as a Lubricant: A Review of the Fundamental Knowledge", Wear <u>10</u> 422-452 (1967).

9. P.J. Bryant, P.L. Gutshall, and L.H. Taylor, "A Study of Mechanisms of Graphite Friction and Wear", Wear <u>7</u>, 118-126 (1964).

10. M.N. Gardos, "Theory and Practice of Self-lubricating Oscillatory Bearings for High Vacuum Application. Part I. Selection of the Self-lubricating Composite Material", Lubrication Engineering <u>37</u>, 641-656 (1981).

11. A.W. Ruff and M.B. Peterson, "Wear Mechanisms in Self-lubricating Metal-matrix Composites" in <u>Tribology of Composite Materials</u>, ed. P.K. Rohatgi, P.J. Blau, and C.S. Yust, ASM International, 43-49 (1990).

12. A.A. Conte, "Graphite Intercalation Compounds as Solid Lubricants," STLE Transactions <u>26</u>, 200 (1983).

13. The $NiCl_2$-intercalated graphite material was obtained from Intercal Co., Port Huron MI.

14. The MoS_2 material was obtained from Cerac, Inc., Milwaukee WI.

15. M.B. Peterson and S. Ramalingam, "Coatings for Tribological Applications", in <u>Fundamentals of Friction and Wear of Materials</u>, ed. D.A. Rigney (ASM International, Materials Park, OH) 1980, pp. 331-372.

16. I.L. Singer, "Solid Lubricating Films for Extreme Environments", in <u>New</u>

Materials Approaches to Tribology: Theory and Applications, ed. L.E. Pope. L.L. Fehrenbacher, and W.O. Winer, Materials Research Society, vol. 140, 215-226 (1989).

17. M.R. Hilton and P.D. Fleischauer, "Structural studies of Sputter-deposited MoS_2 Solid Lubricant Films" in _New Materials Approaches to Tribology: Theory and Applications_, ed. L.E. Pope. L.L. Fehrenbacher, and W.O. Winer, Materials Research Society, vol. 140, 227-238 (1989).

18. E.W. Roberts and W.B. Price, "In-vacuo Tribological Properties of High-rate Sputtered MoS_2 Applied to Metal and Ceramic Substrates", in _New Materials Approaches to Tribology: Theory and Applications_, ed. L.E. Pope. L.L. Fehrenbacher, and W.O. Winer, Materials Research Society, vol. 140, 251-264 (1989).

19. B.C. Stupp in _Thin Solid Films_, _84_, 257 (1981).

20. P.D. Fleischauer and R. Bauer, Tribology Transactions, _31_ 239 (1988).

21. E.W. Roberts in _Tribology - Fifty Years On_, U.K. Inst. Mech. Engs. _1_, 503 1987).

22. Specimens were provided by Ovonics, Inc., Troy MI, through Aerospace Corporation, Los Angeles CA.

23. P. W. Centers, "The Role of Oxide and Sulfide Additions in Solid Lubricant Compacts", Tribology Transactions _31_, 2, 149-156 (1988).

24. Y. Tsuya, Journal Japan Inst. Composites _11_ 127 (1985).

25. S. Fayeulle, P.D. Ehni, and I.L. Singer, "Role of Transfer Films in Wear of MoS_2 Coatings" in _Mechanics of Coatings (Leeds-Lyon Tribology Series)_, ed. D. Dowson, C.M. Taylor, and M. Godet, pp. 129-138, Elsevier (1990).

26. P.D. Fleischauer and R. Bauer, "The Influence of Surface Chemistry on MoS_2 Transfer Film Formation", ASLE Transactions _30_, 160-166 (1987).

27. D.J. Boes, "Solid Lubrication Technology - Part 1 - Solid Lubricated High Speed Ball Bearings", AFAPL-TR-71-69-PT-1, NTIS AD-731163 (Aug 1971).

28. D.J. Boes, "Solid Lubrication Technology - Part 2- Solid Lubricated High Speed Ball Bearings", AFAPL-TR-69-29-PT-2, NTIS AD-880501/2ST (1969).

29. T.M. Yonushonis, "Solid Lubricated Silicon Nitride Bearings at High Speeds and Temperatures", SKF Report AT820002 (1982).

30. R.O. Dayton and M.A. Sheets, "Evaluation of Grooved Solid Lubricate Bearings", AFAPL TR-75-76 (1976).

31. D.E. Brewe, H.W. Scibbe, and W.J. Anderson, "Friction Torque of Ball Bearings with Burnished MoS_2 using Five Retainer Materials", NASA TN D-7023 (1970).

32. R.L. Johnson and H.E. Sliney, "Preliminary Evaluation of Grease to 316C and Solid Lubricants to SiC in Ball Bearings", NASA TN D-4752 (1968).

33. S.F. Murray, P. Lewis, and A.J. Babecki, "Lubricant Life Tests on Ball Bearings for Space Applications", ASLE Transactions 9, (1966).

34. K.R. Mecklenburg, "Material Research on Solid Lubricant Films - Part 1", AFML-TR-67-31 (1967).

35. K.R. Mecklenburg, "Performance of Ball Bearings in Air and Vacuum with No Added Lubrication", AFML-TR-72-73 (1972).

36. C.R. Meeks, "Theory and Practice of Self-lubricated, Oscillatory Bearings for High Temperature Applications - Part II - Accelerated Life Tests and Analysis of Bearings", Lubrication Engineering 37, No. 11, 657 (1981).

37. M.J. Todd and R.H. Bentall, "Lead Film Lubrication in Vacuum", Proc. 2nd. Intern. Conf. on Solid Lubrication", STLE (1978).

38. K.T. Stevens and M.J. Todd, "Parametric Study of Solid Lubricant Composites as Ball Bearing Cages", Tribology Intern. (Oct 1982).

39. R.W. Parcel, as reported in R.I. Christy, "Dry Lubrication for Rolling Element Spacecraft Parts", Tribology Intern. (Oct 1982).

40. D.L. Kirkpatric and W.C. Young, "Evaluation of Dry Lubricants and Bearings for Spacecraft Applications", NASA N69-11810 (Oct 1968).

41. R.D. Brown, R.A. Burton, and P.M.Ku, "Long Duration Lubrication Studies in Simulated Space Vacuum", ASLE Transactions 7 (1964).

Table 1. Applications involving self-lubricating composite materials in a
          different tribological systems.

Application	Element/System
Rolling bearing	Ball/roller retainer
Journal bearing	Journal/sleeve
Hydraulic systems	Sliding seals
Power transmission	Splines, couplings
Consumer products	Bushings, pads
Aerospace systems	Gears, bearings, pads

Table 2. Reported lifetimes for solid lubricated rolling contact bearings.

Name	Bearing Type	Cage Material	Lubricant	Life (x100 MRev)	Ref
Boes	207	WSe2-Ga/N	- -	0.5	27
Boes	207	WSe2-Ga/N	- -	1.2	28
Yonushonis	205	Carbon-graphite	Graphite	- -	29
Dayton	204	WSe2-Ga/N	- -	0.36	30
Brewe	40 mm	Pb plated/steel	Lead	0.54	31
Sliney	20 mm	CaF2/BaF2/steel	CaF2/BaF2	- -	32
Lewis	R4	Ag,Bi,Pb/steel	Ag,Bi, Pb	4	33
Brown	204	MoS2 composite	MoS2, PTFE	10.8	34
Parcel	R3	PTFE composite	PTFE	20.5	35
Mecklenburg	R4	Leaded bronze	Pb	5.1	36
Mecklenburg	204	Leaded bronze	Pb	97	37
Meeks	127 mm	PTFE/glasss/MoS2	PTFE/MoS2	1.2	38
Todd	42 mm	Leaded bronze	Pb	0.08	39
Todd	42 mm	PTFE/glasss/MoS2	PTFE/MoS2	0.08	40
Young	R4	PTFE/glasss/MoS2	PTFE/MoS2	1.7	41

Table 3. Bronze - MoS2 Composite Material for Bearing Retainers

Description:

A bronze - MoS2 composite material has been fabricated and tested in sliding against bare 440C steel rings or alternatively against sputtered MoS2 coatings on 440C steel rings. The composite was produced by infiltrating a MoS2 - ethanol mixture into porous bronze (90 copper - 10 tin) by a vacuum technique. The composite can be cold-pressed after infiltration to increase its strength. The starting bronze material was about 60 % dense, and had nominal pore sizes of either 20, 30, or 50 μm. A laboratory pin-on-ring test system was used.

Infiltration Method:

Material	- Bronze filter disks, 20 μm pore size (Arrow Pneumatics Inc., 7650 Industrial Drive, Forest Park IL 60130)
	- Molybdenum disulfide (Cerac Inc., 407 N. 13 St., Milwaukee, WI 53233)
Procedure	- Machine the part to nearly final dimensions
	- Open surface pores damaged by machining by immersing the part in 10% HNO3 solution (time to be determined by trial)
	- Ultrasonically agitate in water/detergent solution until all residue is removed
	- Ultrasonically agitate in water for 5 min
	- Ultrasonically agitate in ethanol for 5 min
	- Prepare a beaker containing a solution of 35 g MoS2 per 15 ml ethanol of sufficient quantity to fully immerse the part; agitate the solution ultrasonically for 15-30 sec to suspend the MoS2 particles; immediately place the part in the solution
	- Place the beaker containing the solution and the part in a vacuum vessel; evacuate the vessel and hold for 5 min
	- Release the vacuum, remove the part, and air dry for 10 min
	- Repeat the impregnating and drying steps twice more
	- Final air drying in an oven at 75-100 C for 8-12 hours
	- Burnish the outer surface with additional MoS2 prior to use (removing any excess powder with an air jet)
	- Note: if possible, mechanical compression of the part can be carried out prior to the burnishing step to increase the part strength (by closing any remaining pore volume)

Table 4. Materials Studied in Sliding Against MoS$_2$ Coatings

MATERIAL	SELF-LUBRICATING	COMPOSITION (WT. FRACTION)
Gold	-	Au
Gold-Nickel	-	0.998 Au, 0.002 Ni
Nickel	-	Ni
Molybdenum	-	Mo
Titanium	-	Ti
Copper	-	Cu
80Cu-20I.G.	SL	0.8 Cu, 0.2 intercalated graphite(NiCl2)
Bronze	SL	0.8 Cu, 0.1 Sn, 0.1 Pb
90Bronze-10MoS$_2$	SL	0.72 Cu, 0.09 Sn, 0.09 Pb, 0.1 MoS$_2$
PTFE (Amicon)*	SL	0.8 PTFE, 0.15 glass, 0.05 MoS2
Polyimide (SP3)*	SL	0.85 polyimide, 0.15 MoS2
Polyimide (SP1)*	-	polyimide
Polyimide (SP211)*	SL	0.75 polyimide, 0.1 PTFE, 0.15 graphite
PTFE (Duroid)*	SL	PTFE, glass, MoS2

* Commercial materials are identified in order to provide a complete description.

21

Table 5. Gold-Nickel Alloy Plating for Bearing Retainers

Description:

The plating has been tested for wear and friction performance in a
laboratory pin-on-ring sliding test. The plating was deposited by
electrodeposition on a steel substrate to a thickness of about 0.5-
1 mils (12-25 μm). It was tested against pre-deposited MoS2 coatings on
440C steel rings.

Plating Method:

Electrolyte - Gold @ 12.1 g/L of potassium gold cyanide
            - Nickel @ 0.15 g/L nickel metal in a proprietary
              solution (Autronex Nickel, Sel-Rex OMI, Nutley NJ)
Temperature - 33 C
pH   - 4.0
Current density - 110 A/m^2
Deposition rate - 2.5 μm per 10 min
Agitation - yes
Anodes   - Platinum or stainless steel
Substrate preparation - Degrease in ethanol, acetone, ethanol
                - water rinse, soak in detergent @ 70 C, 5 min
                - water rinse, dip in 5 % H$_2$SO$_4$ for 10 s
                - water rinse, place in plating solution with
                  potential applied, for time duration   required
                - remove, water rinse, dry

Table 6. MoS_2 Vacuum Deposited Coatings Studied – on 440C Rings

Type	Manufacturer	Deposition Method	Date Deposited
DCS	Hohman	DC sputtered	June 1989
RFS	Aerospace-1	RF sputtered, Run #1	Sept. 1989
RFS	Aerospace-2	RF sputtered, Run #2	Sept. 1989
MGS	National Center for Tribology	Magnetron sputtered	Apr. 1990
MLS	Ovonics	Ni/MoS_2 multilayer	Dec. 1990
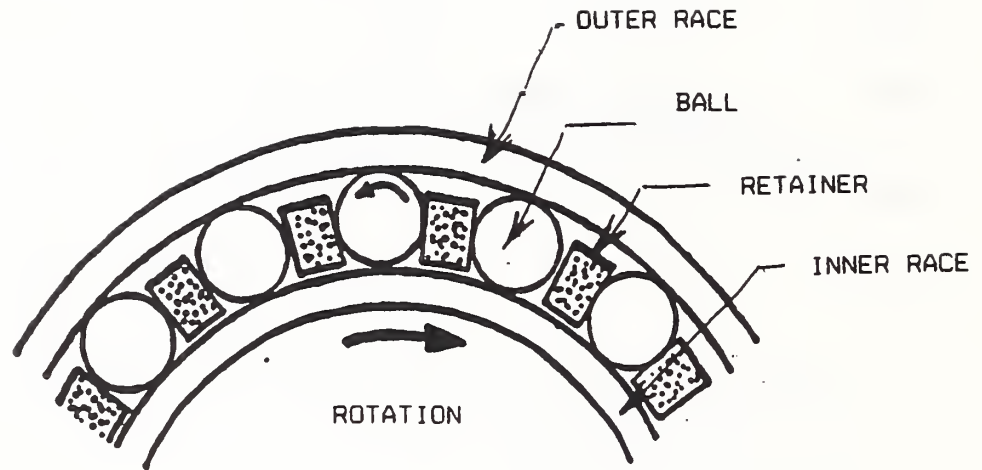
Fig.1   Schematic of a portion of a partial complement bearing with bearing elements indicated.
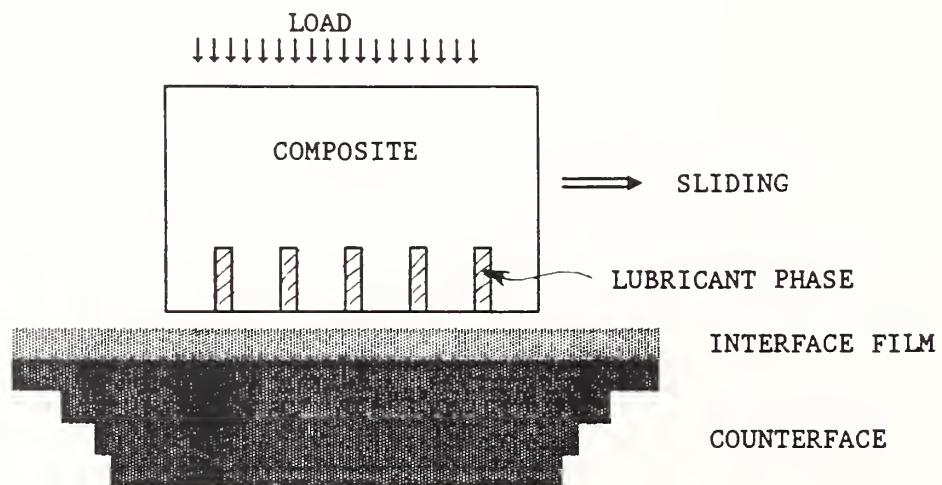
Fig. 2   Schematic of a composite material [retainer] interacting with a solid lubricating interface film on a counterface [race or ball] during sliding motion.
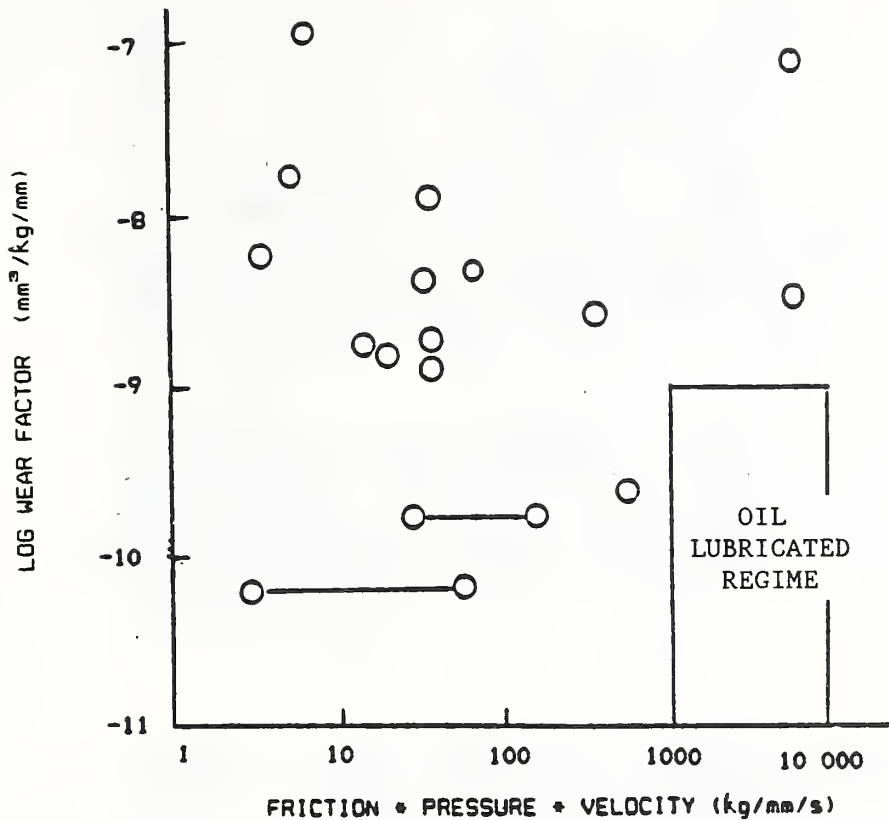
Fig. 3   Wear rates of a variety of solid lubricant materials from bench
          tests under different conditions of load and speed, compared to
          typical wear rates of metallic retainers tested under oil lubricated
          conditions typical of a rolling contact bearing (assuming boundary
          lubrication).
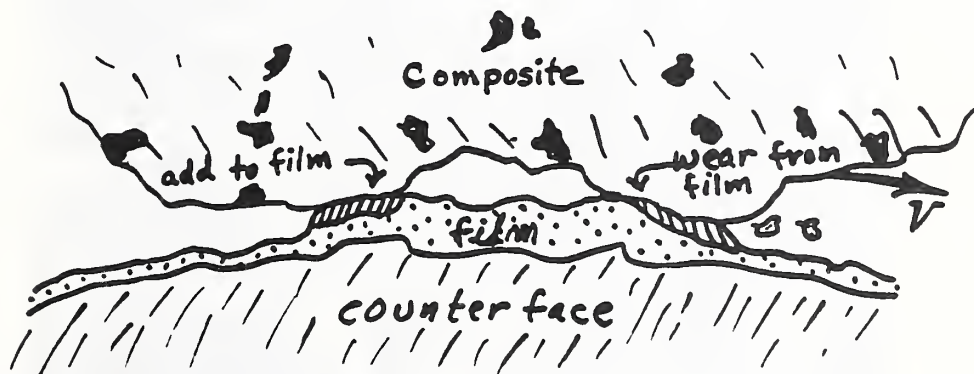
Fig. 4   Schematic illustration of the concept of a dynamic solid lubricating
          film where the film on the counterface [race or ball] is continually
          undergoing changes.

25
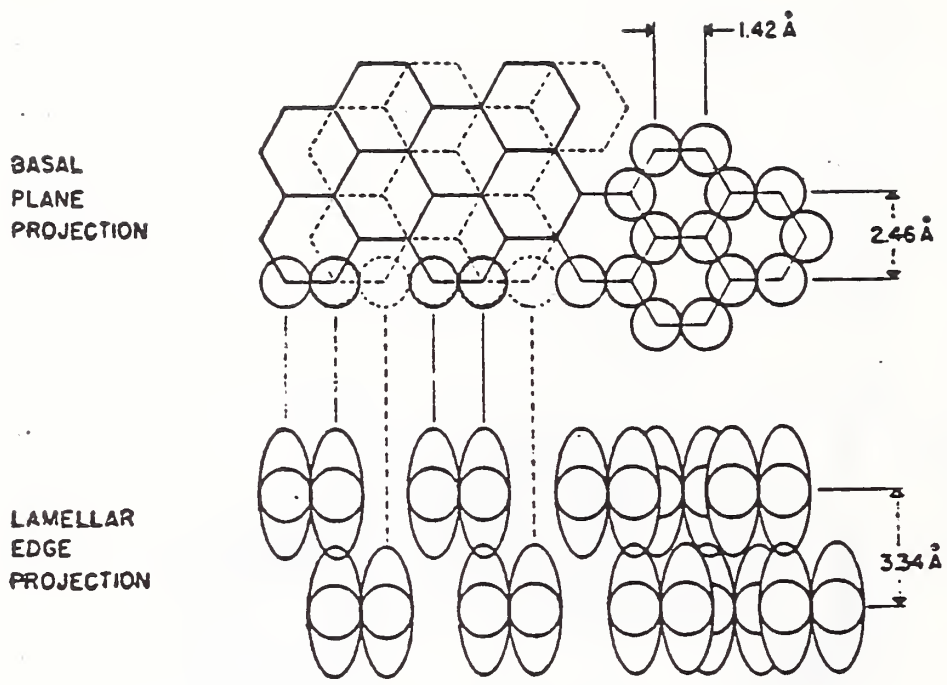
Fig. 5   Schematic drawing of the basal and edge projections of atom positions in graphite.

Fig. 6.   SEM photograph of the morphology of the $NiCl_2$ - IG particles.
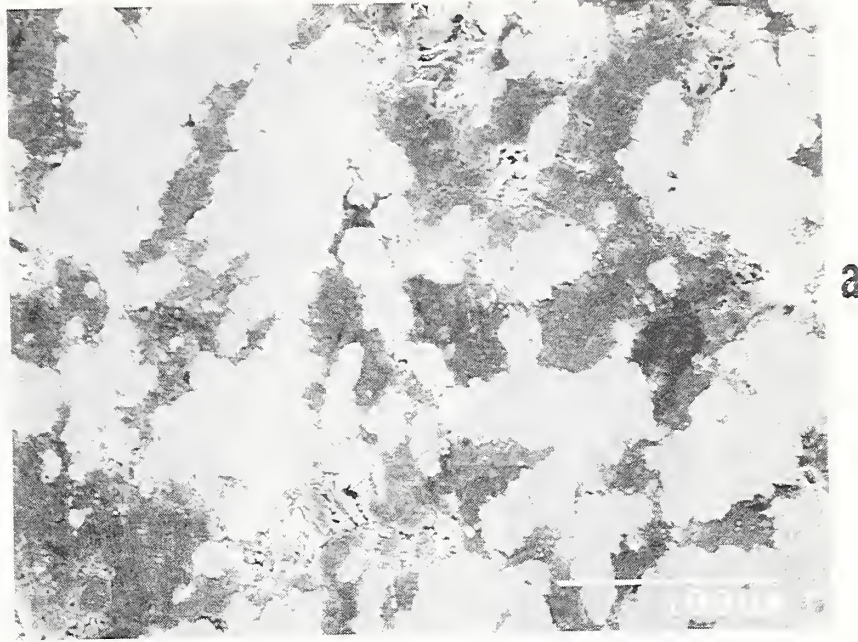
Fig. 7. Photographs of (a) Cu- 57 vol. % IG, and (b) Cu - 20 vol. % IG powder compacted specimens.
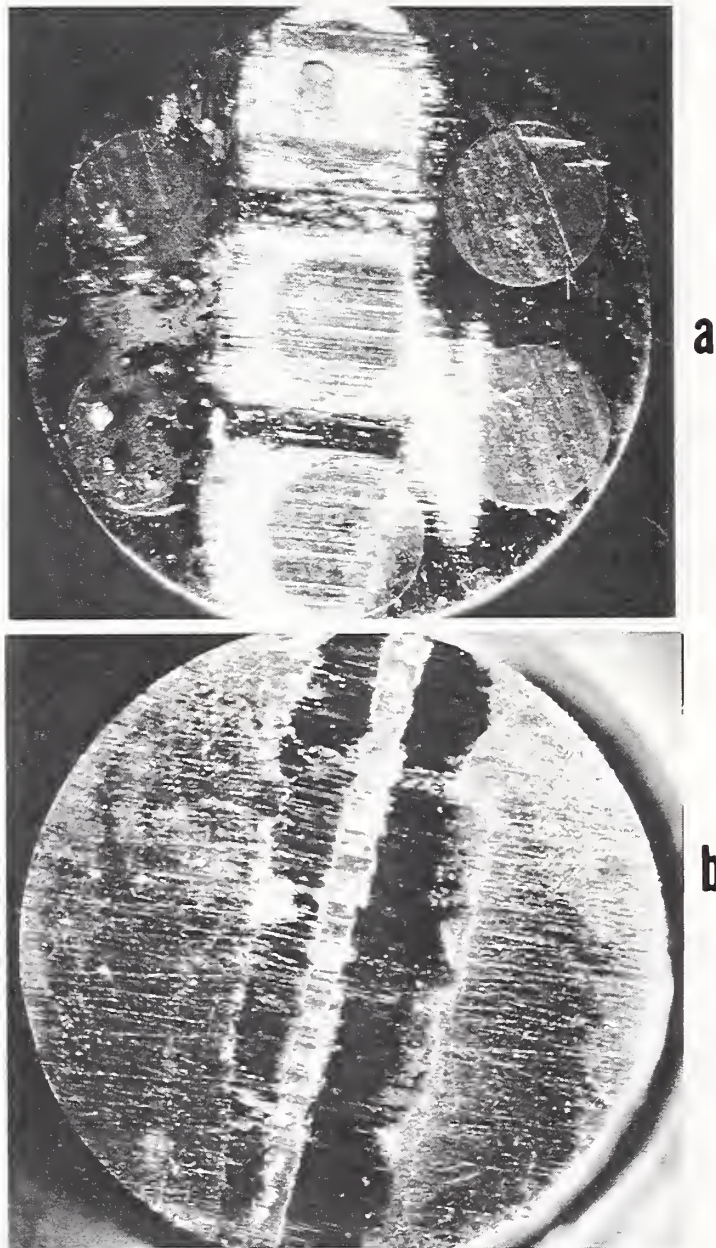
Fig. 8 . Optical photographs of two manufactured Cu - IG composite specimens
after testing showing wear scars and specimen geometries.
(a) Cu-43 vol. % IG; drilled holes contain compacted IG powder.
(b) Cu- 25 vol. % IG; machined slit contains compacted IG powder.
Hole size, hole separation, and slit width were varied to change
effective vol. percent IG.
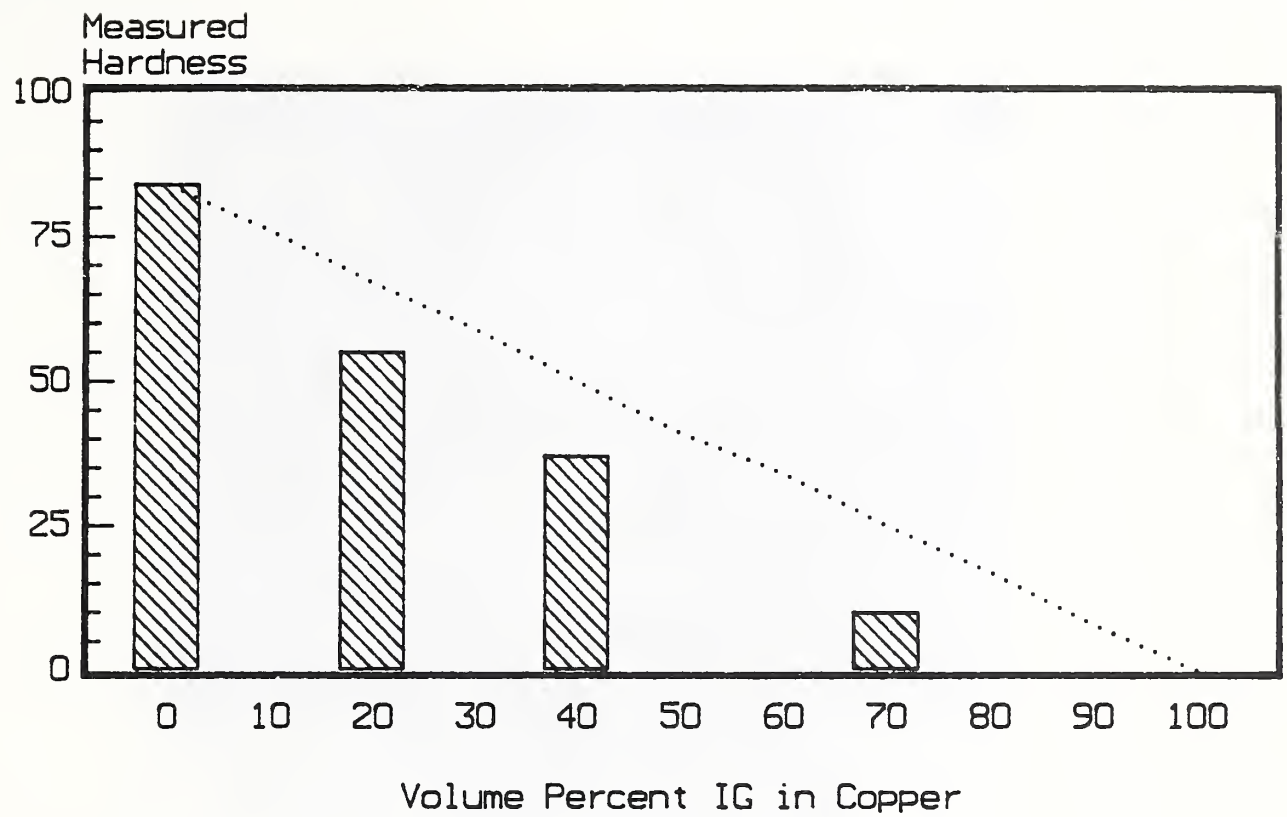
Fig. 9   Measured Rockwell scale 15T superficial hardness values for the Cu-IG composites. The dotted line represents a linear rule-of-mixtures relationship.

a

b

Fig. 10   Microstructure of NIST-prepared bronze- 10 vol. % MoS$_2$ composite.
Optical micrographs of polished surfaces prior to testing.   (a) M =
210 X, (b) M = 420 X.
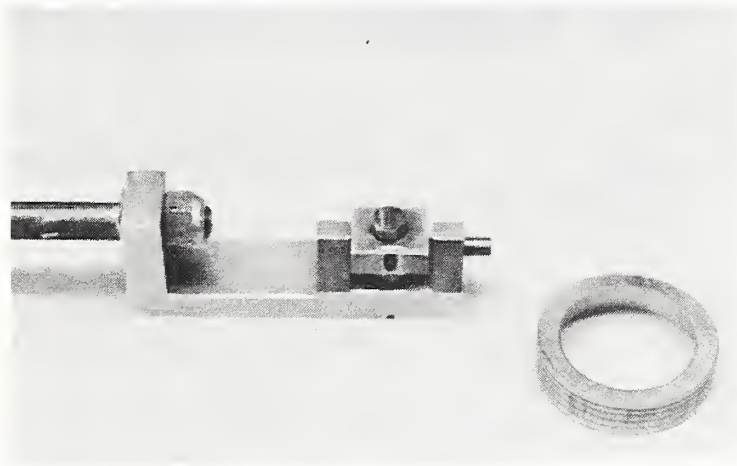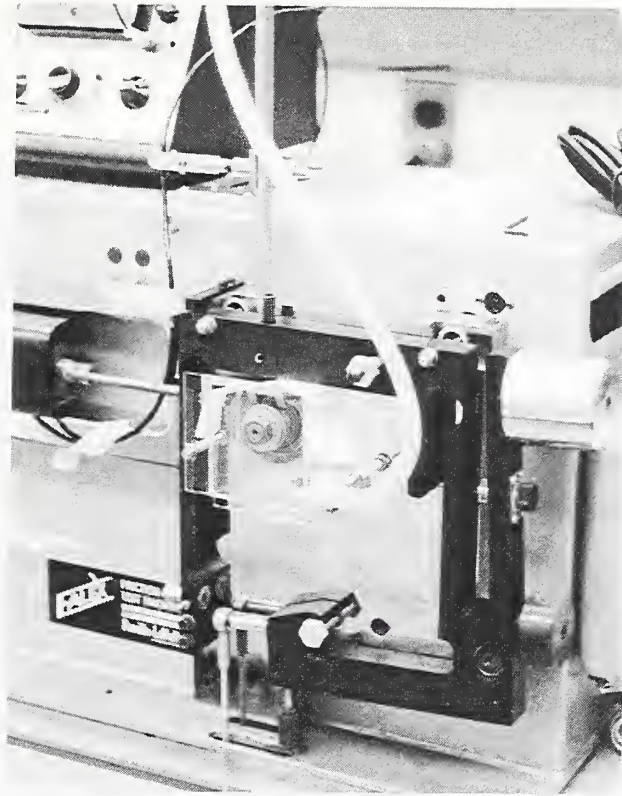
Fig. 11   Photographs of the pin-ring wear test system, with the argon
environment enclosure in place, and the specimen holder and ring.
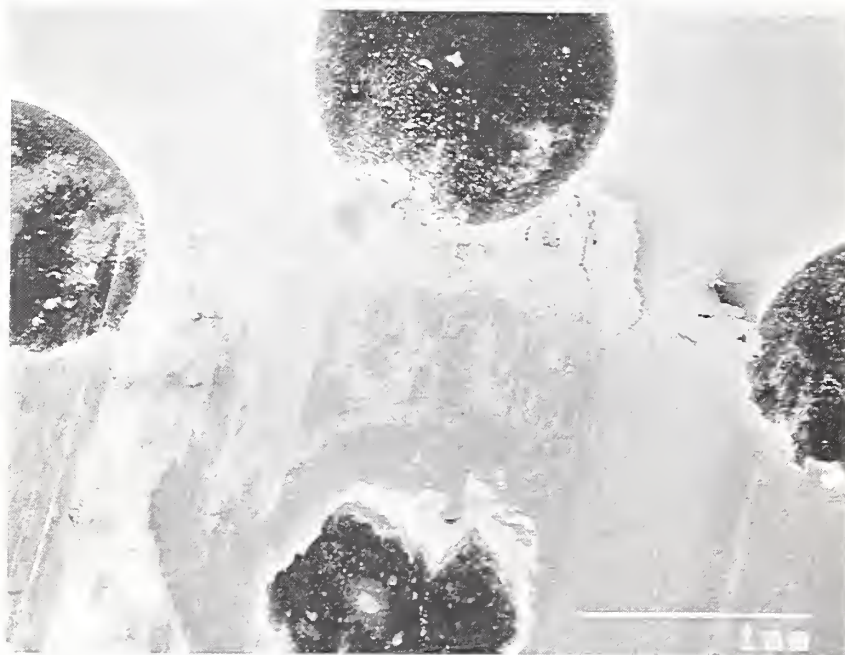
Fig. 12   SEM micrograph of a portion of the wear scar on a manufactured Cu-IG composite.   The interfacial film within the scar can be seen.
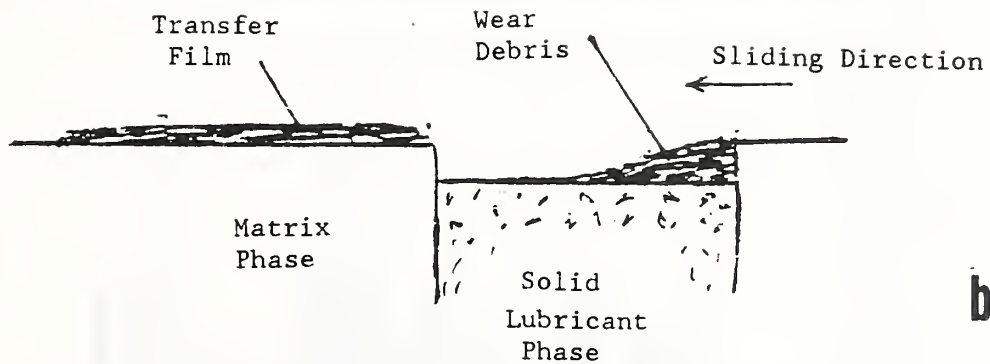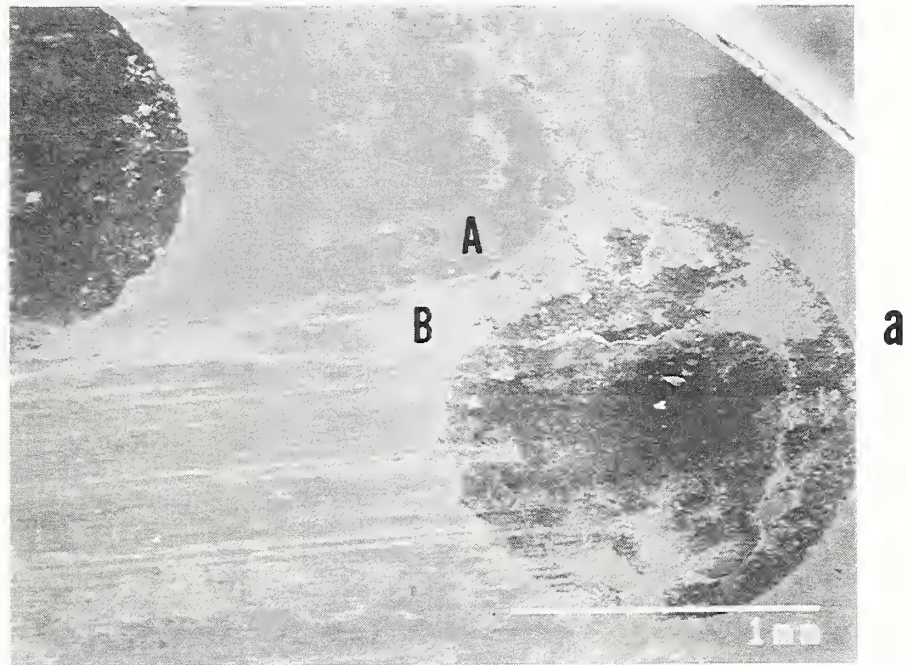
Fig. 13 (a) SEM photograph of worn area in Cu-25 vol. % IG composite.
Sliding direction is right to left. Wear debris is collected at
the entrance edge of the recessed IG region. Interfacial film is
formed at the exit edge of the IG region; film thickness varies
with location (A and B). (b) Cross-section sketch of the detail
near an IG region; soft phase recession depth was typically 1-5
μm.
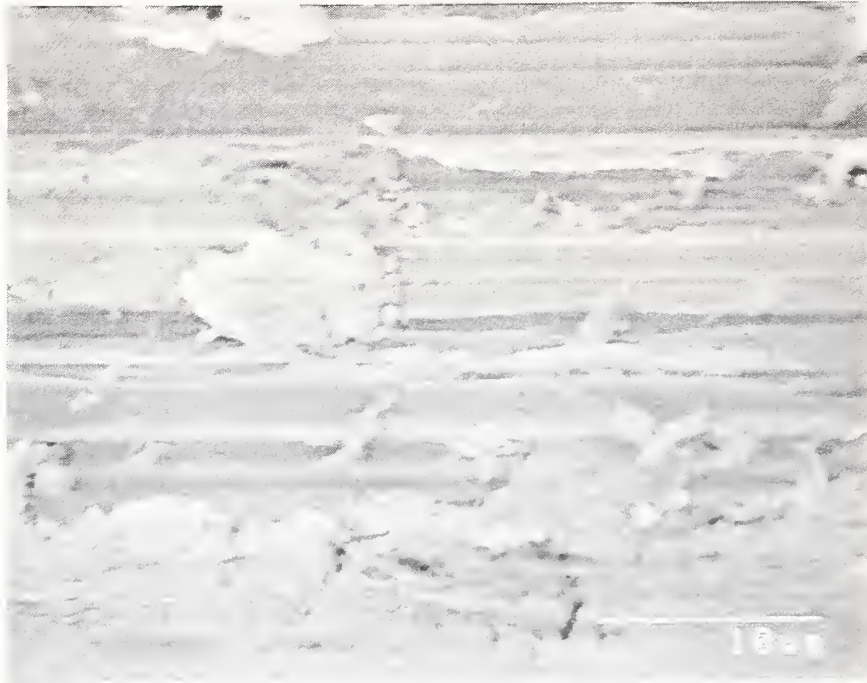
Fig. 14   SEM micrograph of a worn surface on a 440C steel ring showing the patchy interfacial film.
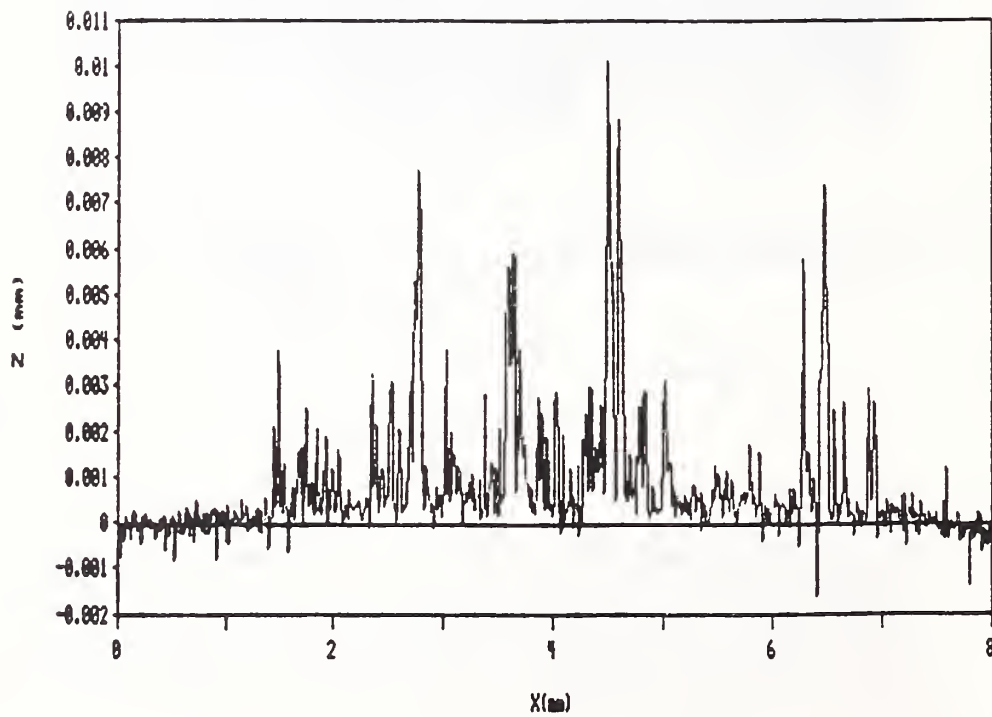
Fig. 15   A stylus profile recording of the interfacial film on a 440C steel ring is shown indicating the variation of thickness of the film patches.
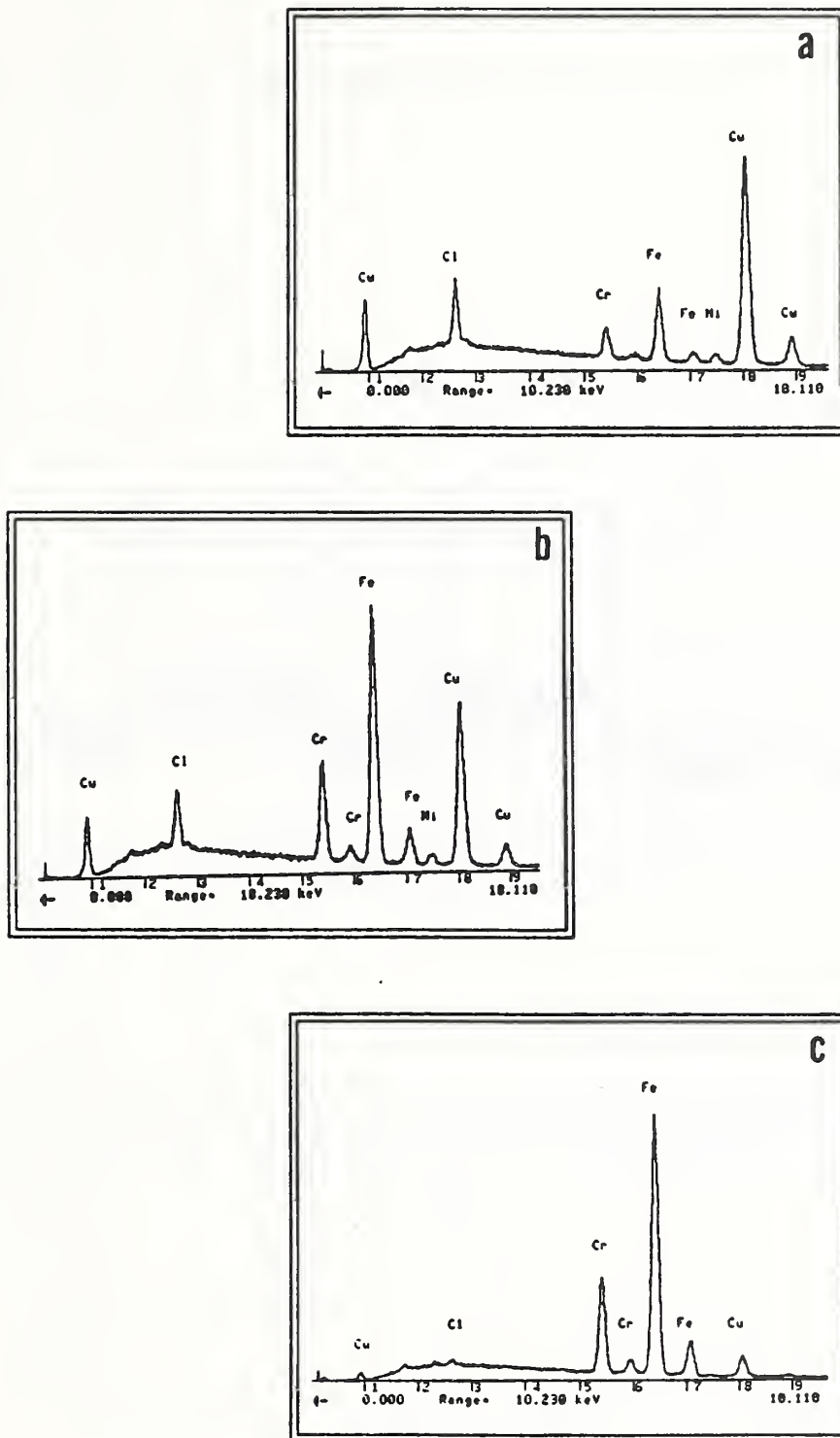
Fig. 16   X-ray spectra from three different film regions: (a) the film
          region is on the composite pin, from a region overlaying the copper
          matrix, immediately at the exit side of an IG phase region; (b) the
          film region is on the composite pin, well removed from any IG phase
          region;   (c) the film region is from the steel ring surface.
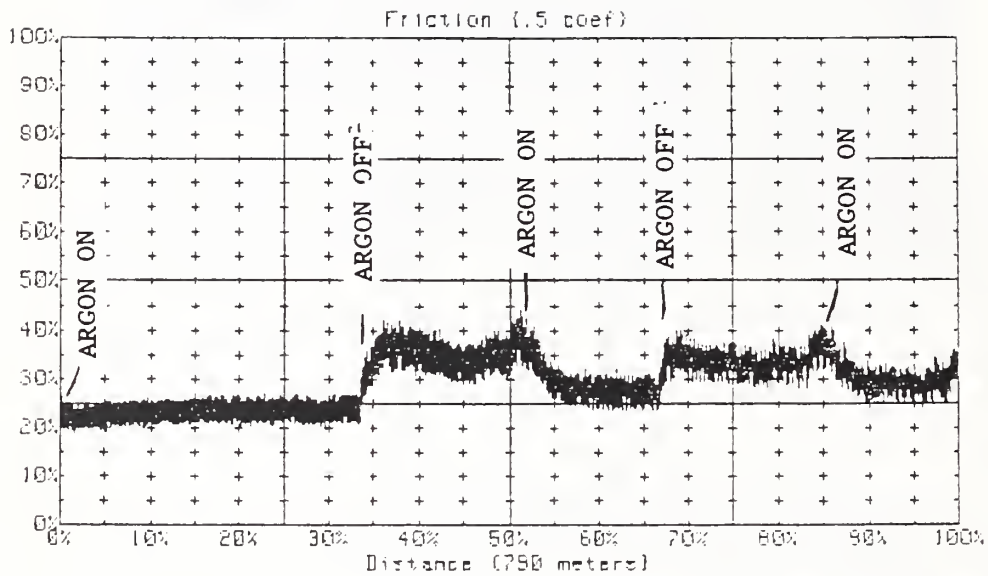
Fig. 17   Friction coefficient vs sliding distance for a test of Cu - 57 vol.
% IG specimen against 440C steel showing the effect of interrupting
the argon supply to the test chamber on two occasions, allowing lab
air to infiltrate into the test atmosphere.
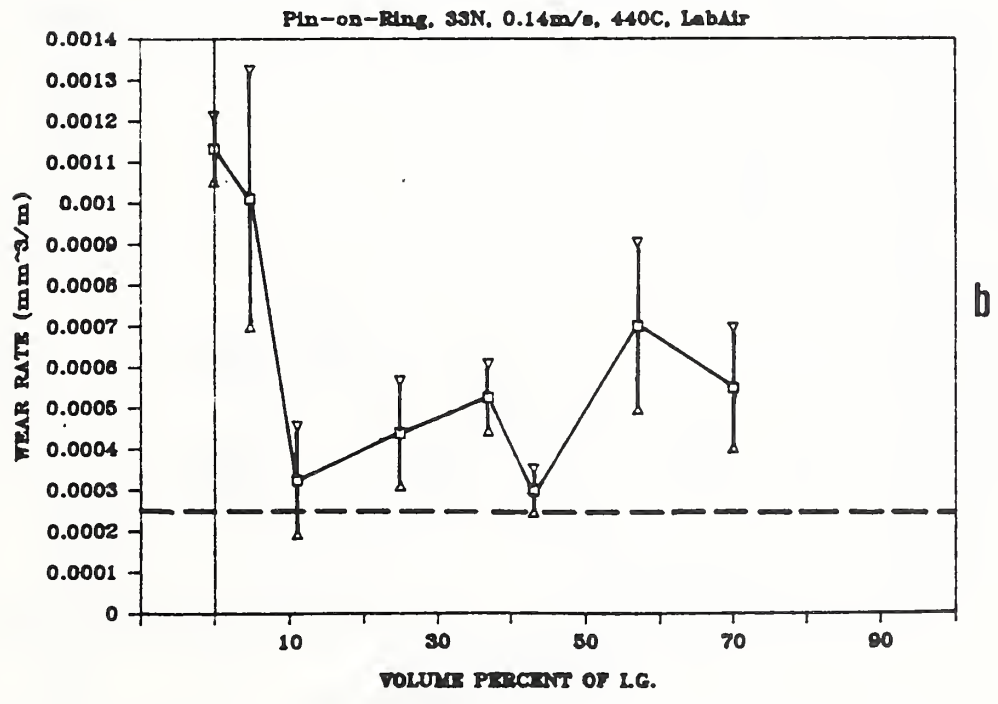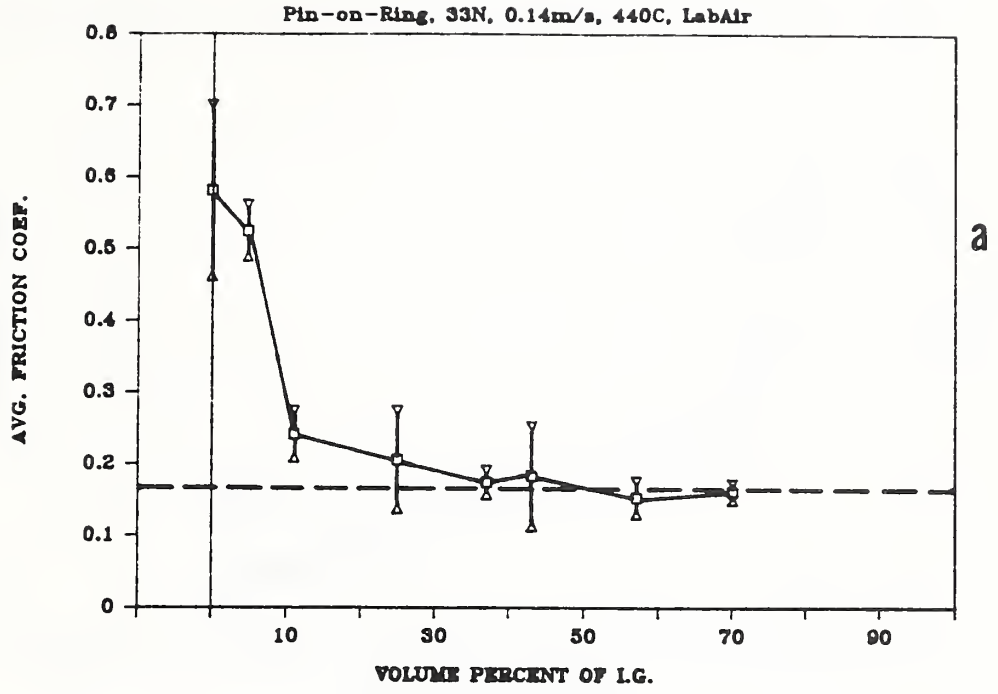
Fig. 18 (a) Friction coefficients for the Cu - IG composites in lab air. Dashed line represents baseline for 2-pin tests. Range of ± std. dev. shown for each average value. (b) Wear rate results for Cu - IG composites. Dashed line represents wear rate baseline from 2-pin tests.
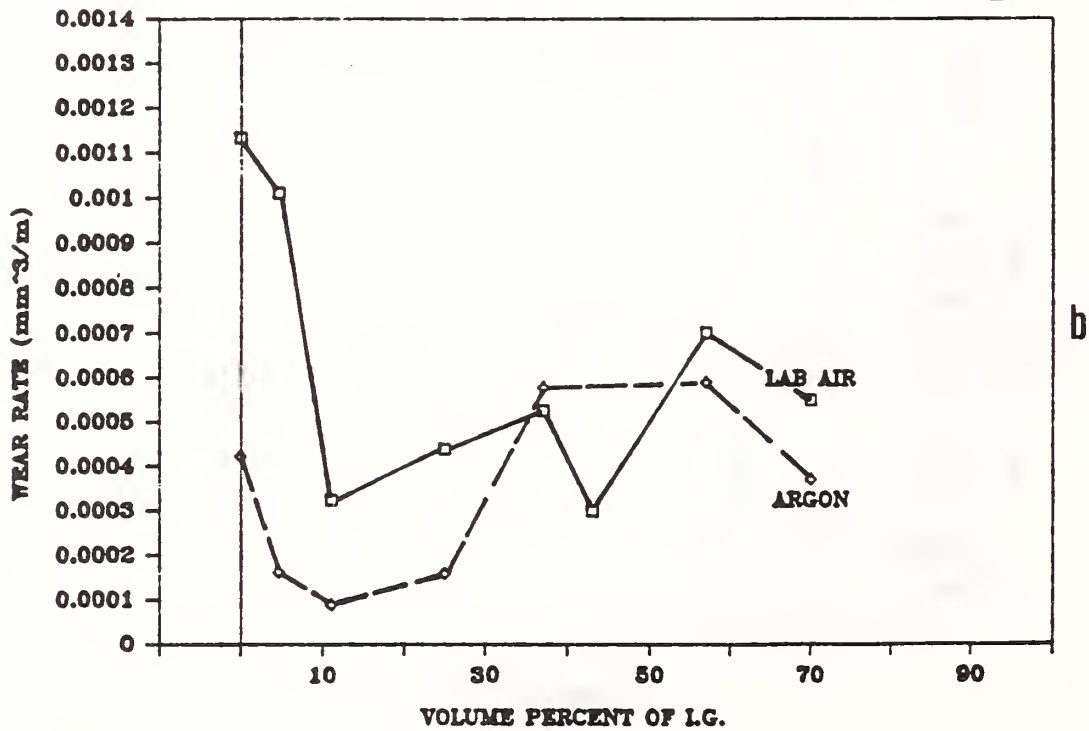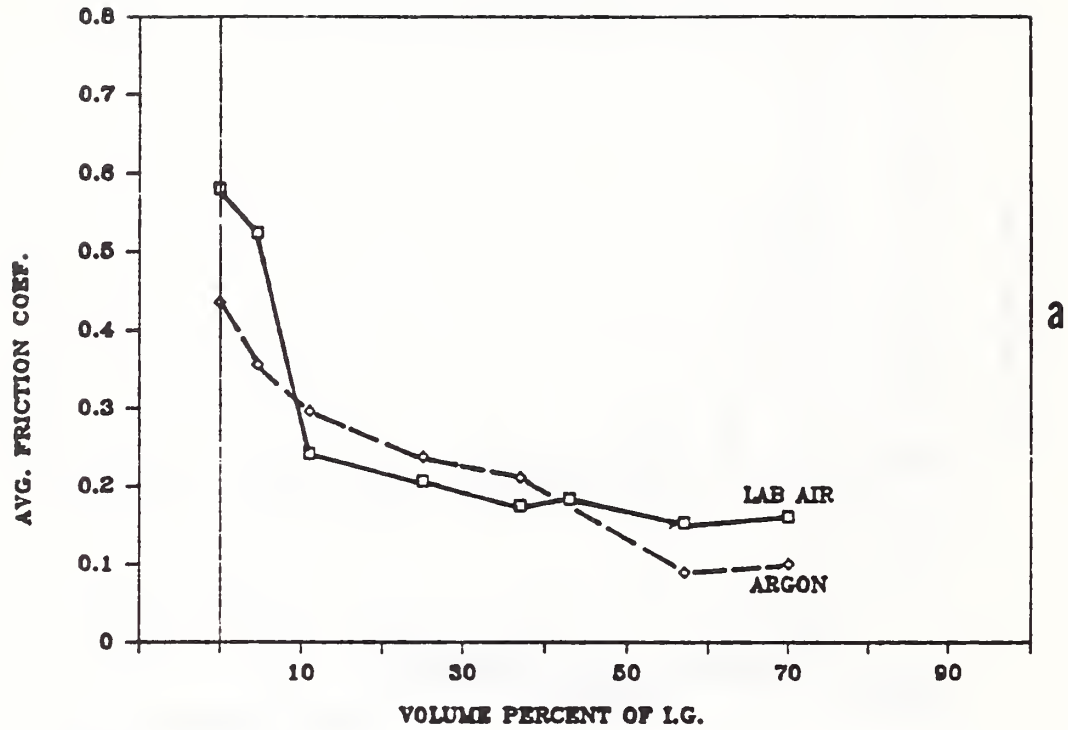
Fig. 19   (a) Comparison of friction coefficients for the Cu - IG composites
tested in air and in dry argon.   (b) Comparison of wear rate
results.
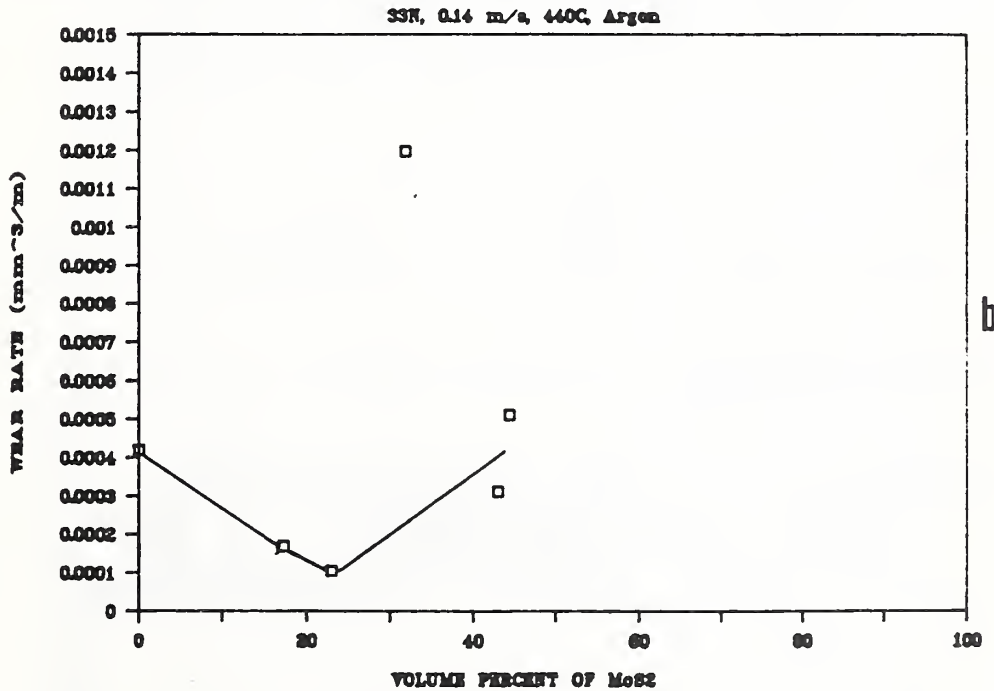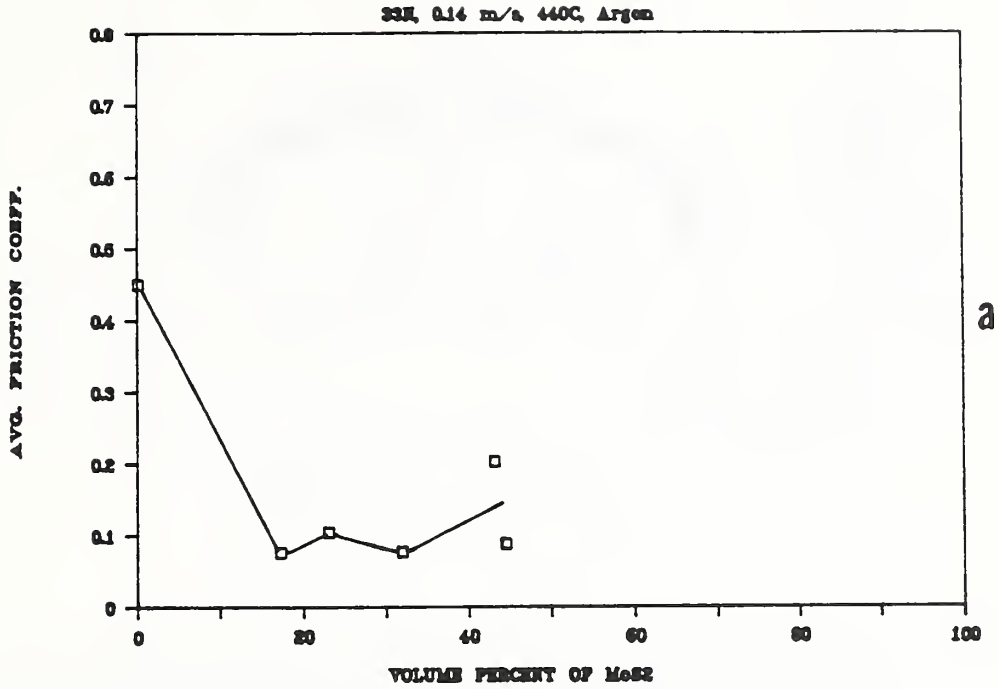
Fig. 20 (a) Friction coefficients and (b) wear rate results for the bronze -
MoS_2 composites in argon.

39
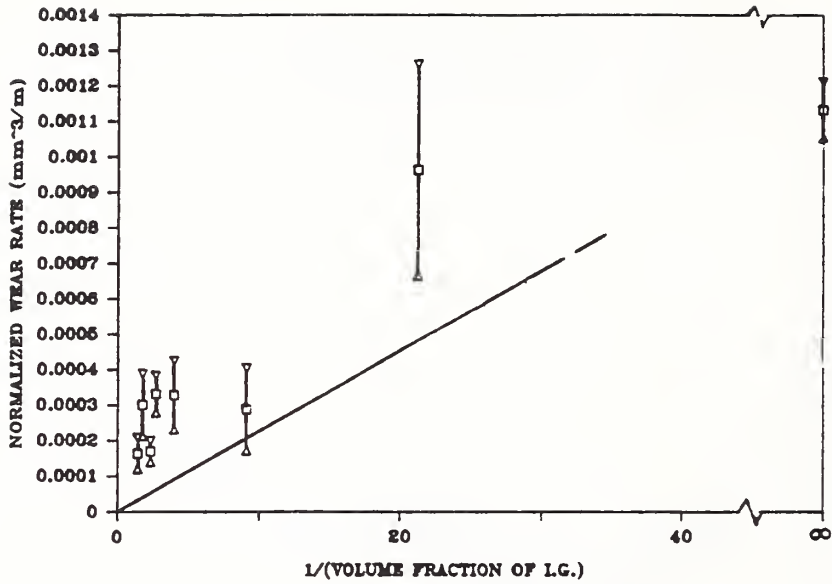
Fig. 21   Comparison of model prediction with wear data (normalized by vol. percent Cu). Solid line describes ideal wear of composite to maintain interfacial film at constant thickness.
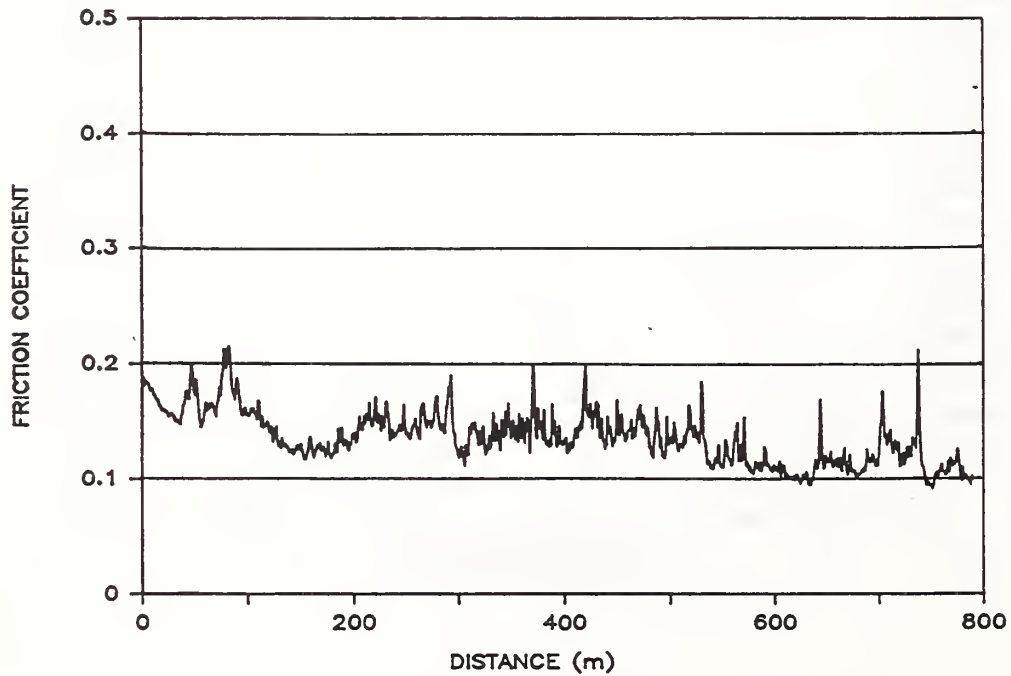
Fig. 22   Friction _vs_ distance results for a 2-pin test, bronze and MoS_2 pins, sliding against a 440C steel ring for 800 m under 33 N load in argon. The slow trend to establish a stable interfacial film can be seen, along with brief variations to higher and to lower friction values, depending on local conditions.
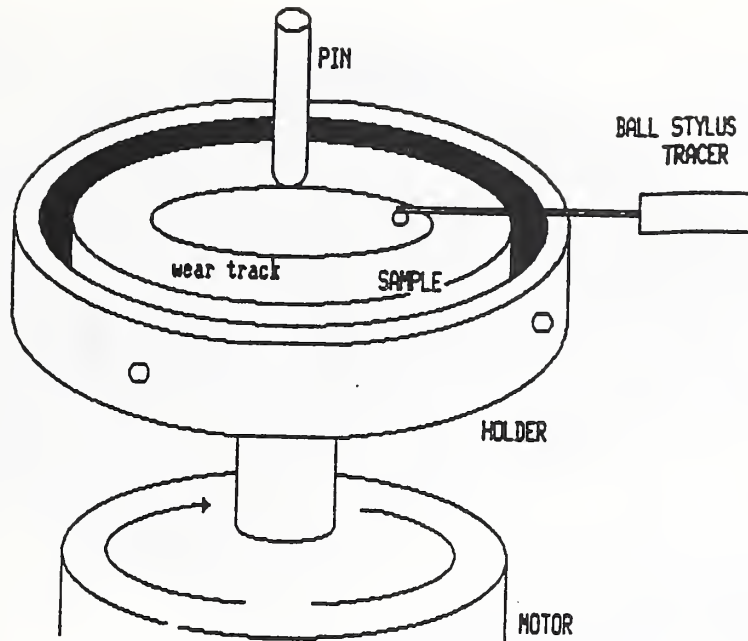
Fig. 23   Schematic drawing of pin-on-disk tribometer used to create graphite and MoS$_2$ films by sliding.   A ball-stylus profiling tracer was used to measure interfacial film thickness and topography during interruptions of the disk rotation.
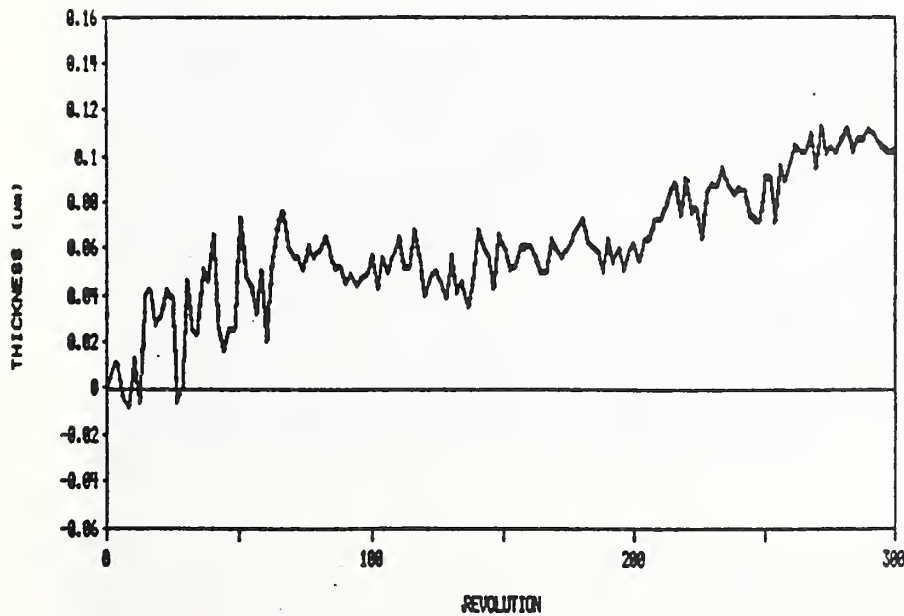
Fig. 24   MoS$_2$ film average thickness vs revolution number for a film produced on type 52100 bearing steel in dry argon using a 1.7 N load in the apparatus shown above.
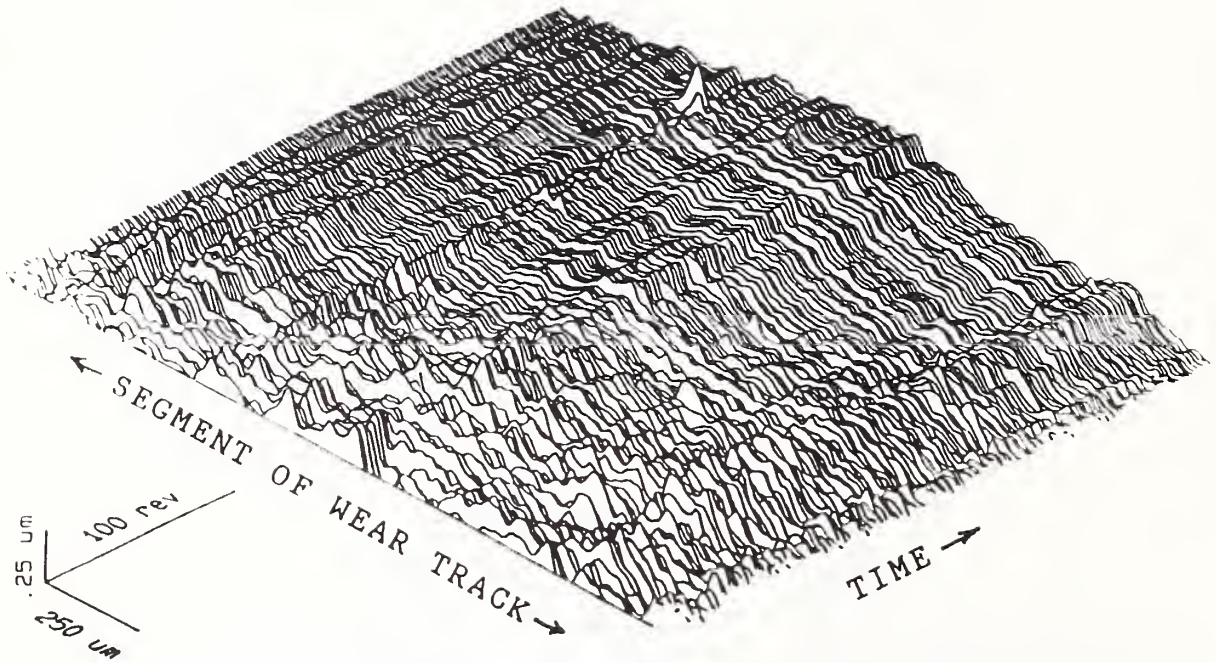
Fig. 25   Profile of an MoS$_2$ film traced across the wear track for the first
           300 cycles of sliding, plotted <u>vs</u> time (cycles) as the film forms.
           Note the appearance and disappearance of several features in the
           film topography as its thickness gradually increases.

Fig. 26   Morphology of as-deposited type MGS coating of MoS$_2$ on 440C steel
           ring prior to testing.
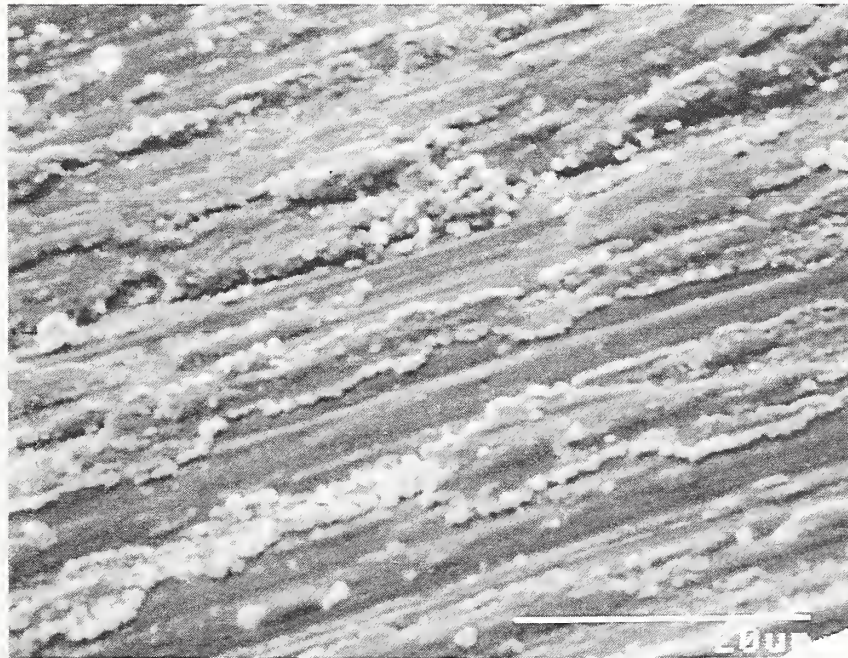
Fig. 27   SEM micrographs from a 1900 m test in lab air on a RFS type coating
using a Cu - 20 vol. % IG pin. Detail of the coating damage is seen
in the lower photograph.

Fig. 28   SEM micrographs from a 1900 m test in dry argon on a RFS type
           coating using a Cu - 20 vol. % IG pin. Much less coating damage is
           seen.
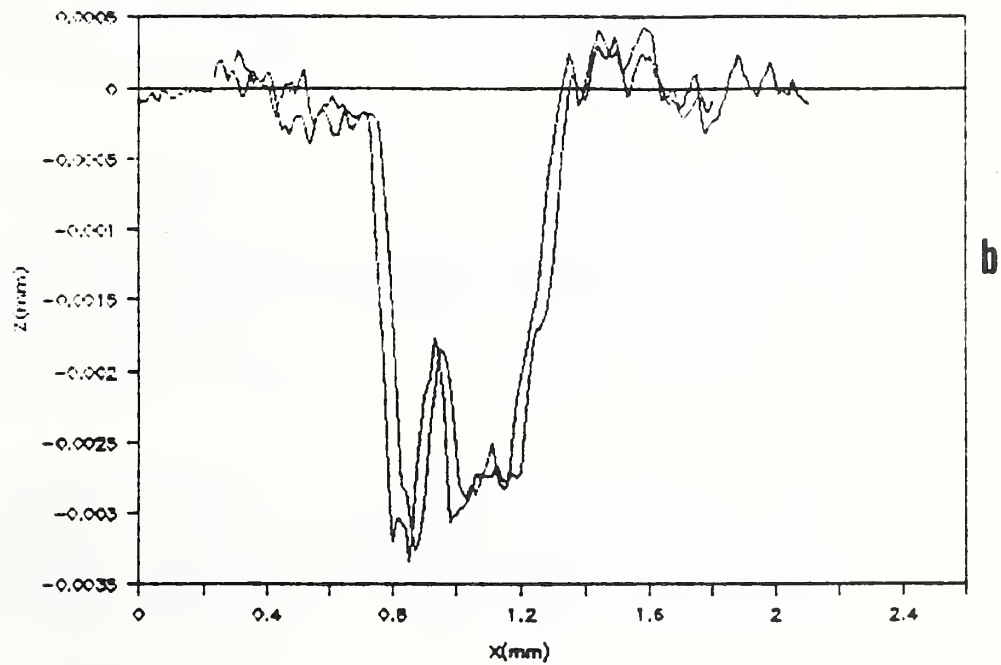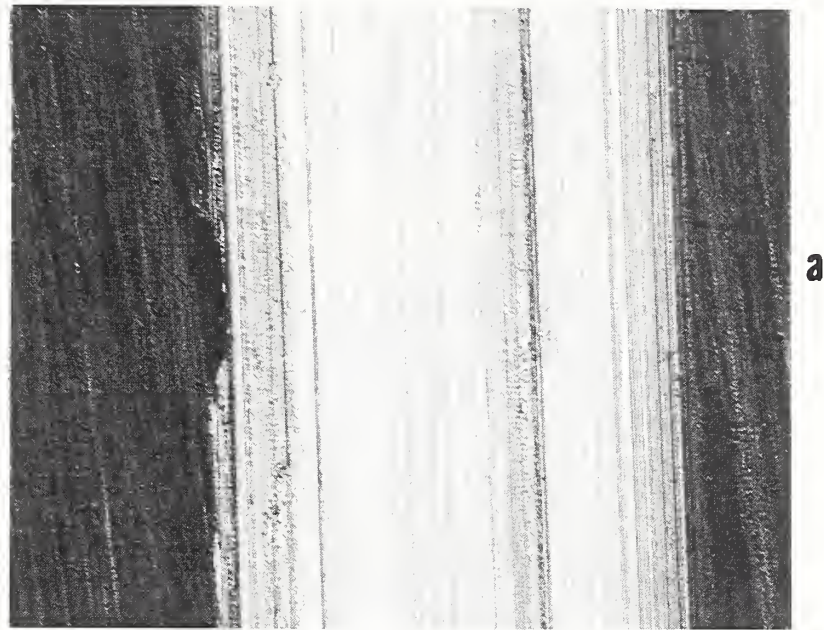
Fig. 29   Appearance of wear track on type MGS coating after test with Au
           specimen: (a) optical micrograph, M = 105 X, (b) stylus profile
           across wear track in one location.
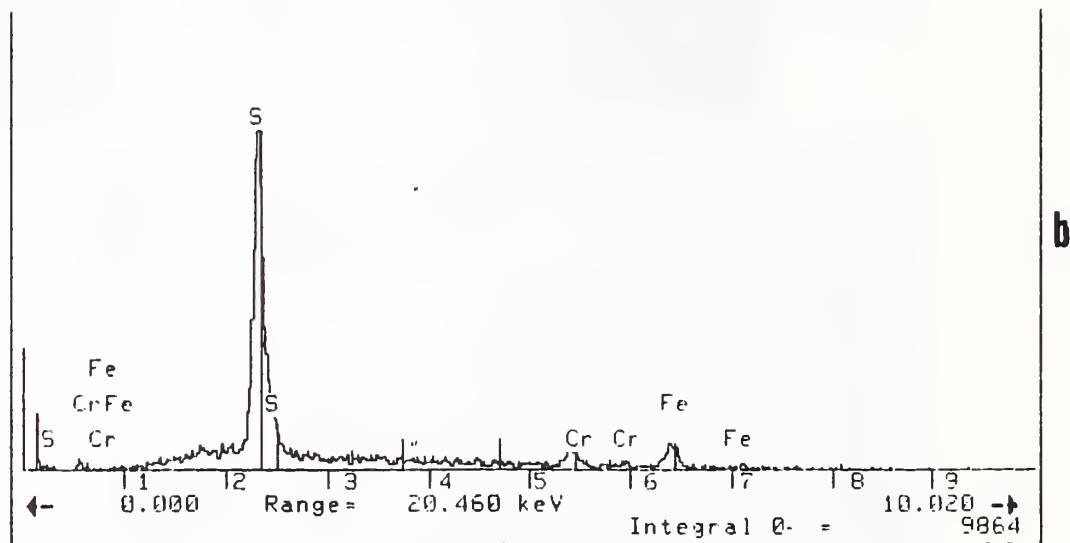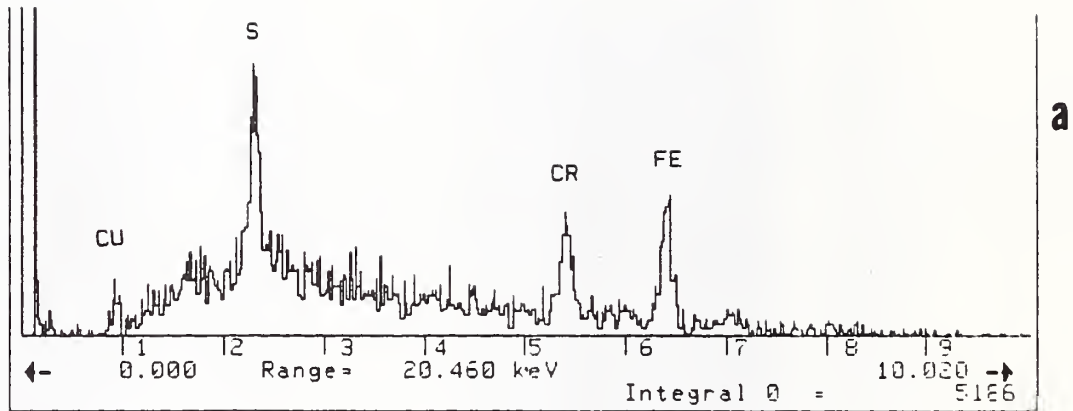
Fig. 30   EDX analyses from worn regions on two type RFS coatings after 1900 m
sliding tests using Cu-IG specimen (a) in air, (b) in dry argon. The
incorporation of copper and steel wear debris in the coating is more
extensive when sliding in air, but is present in both cases.

ARGON   LAB AIR
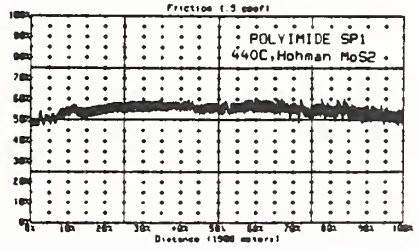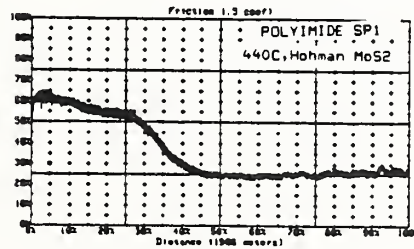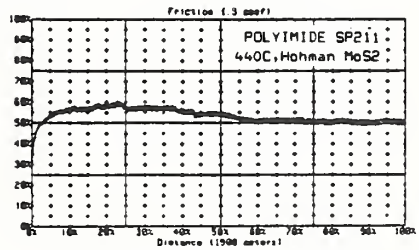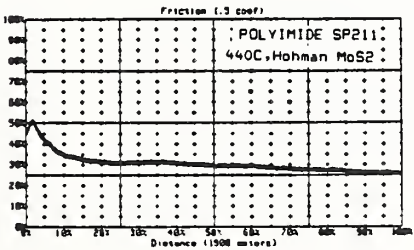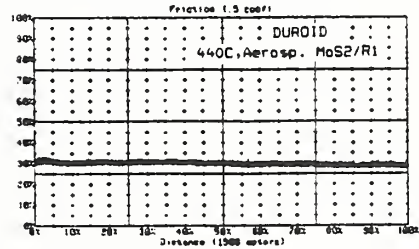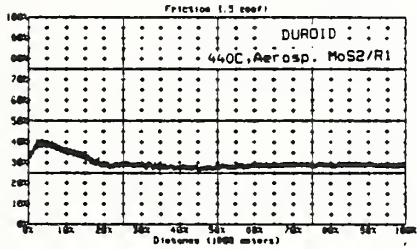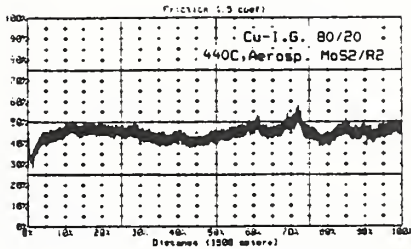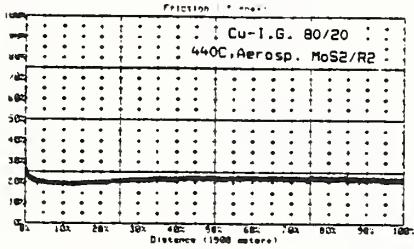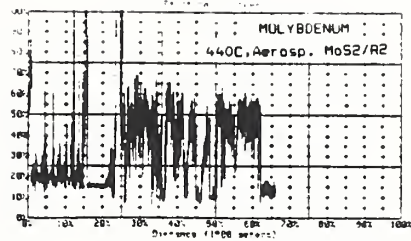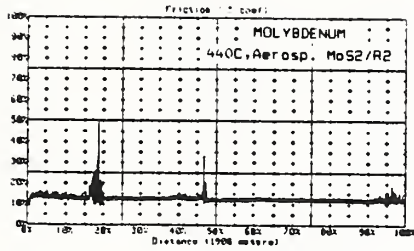
Fig. 31   Friction vs. distance results for several material-coating
          combinations in either dry argon or air test environment.
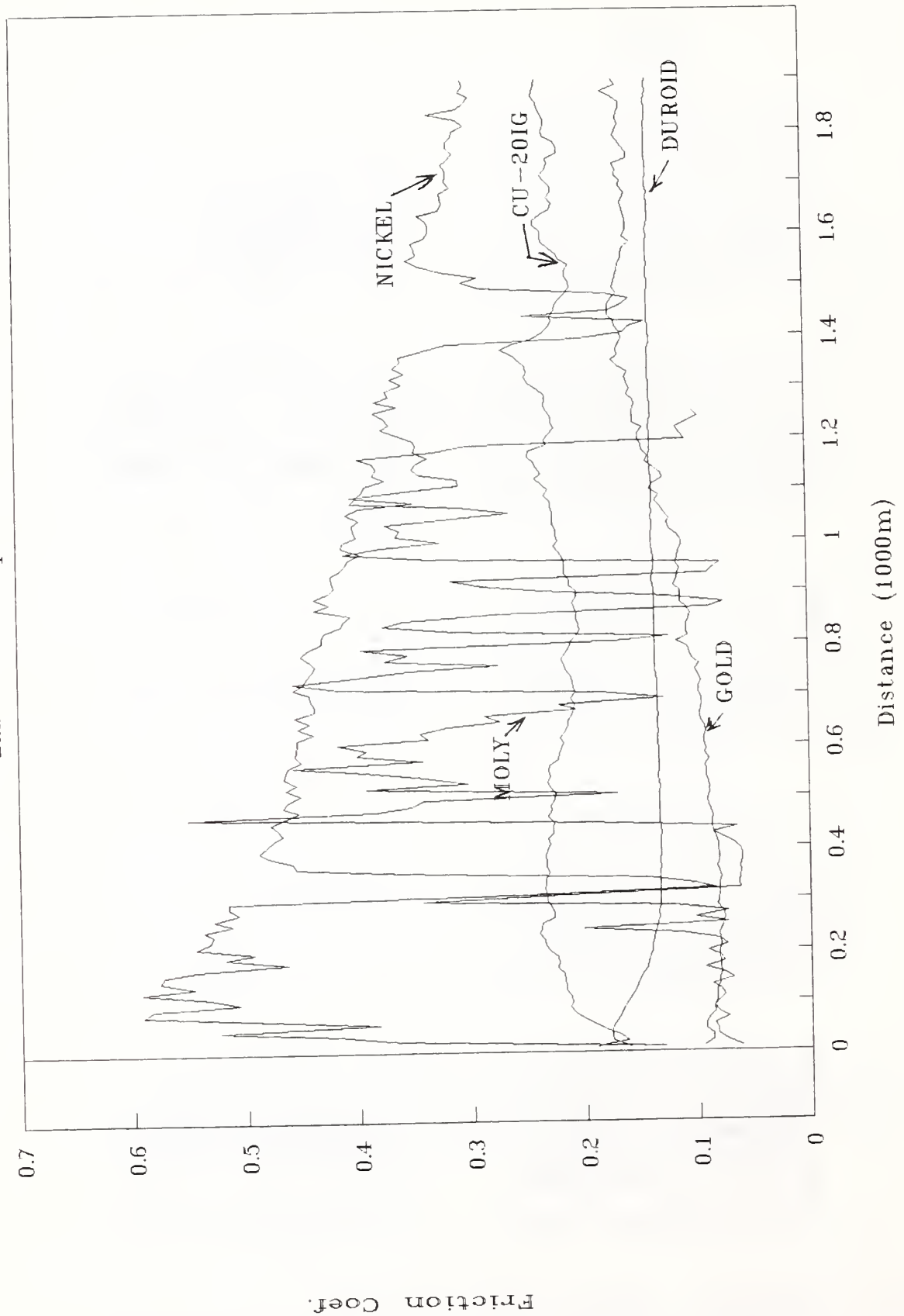
Fig. 32 Friction coefficient vs. sliding distance for 5 materials on type RFS MoS_2 coating in lab air.
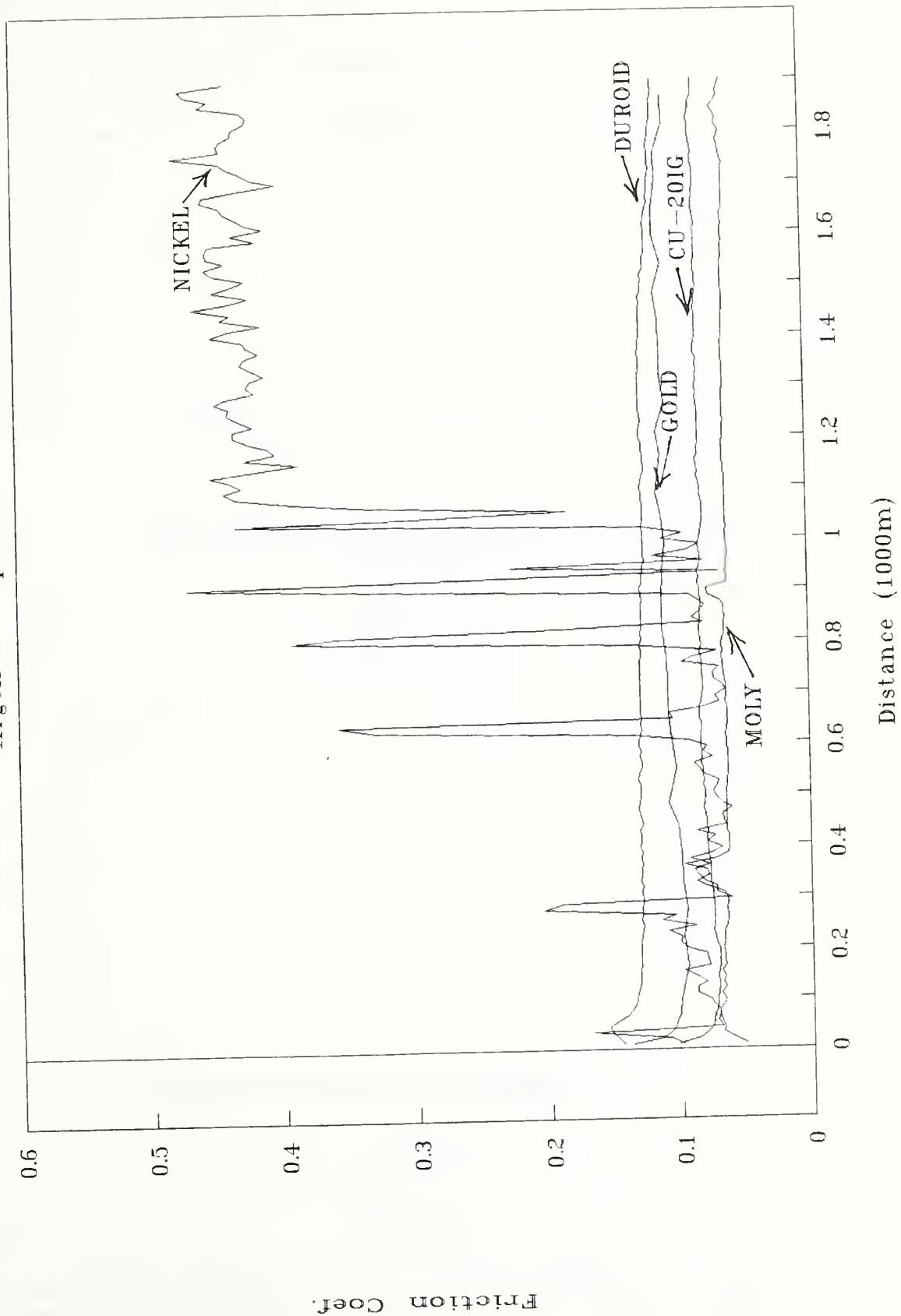
Fig. 33 Friction coefficient vs. sliding distance for 5 materials on type RFS MoS$_2$ coating in argon.
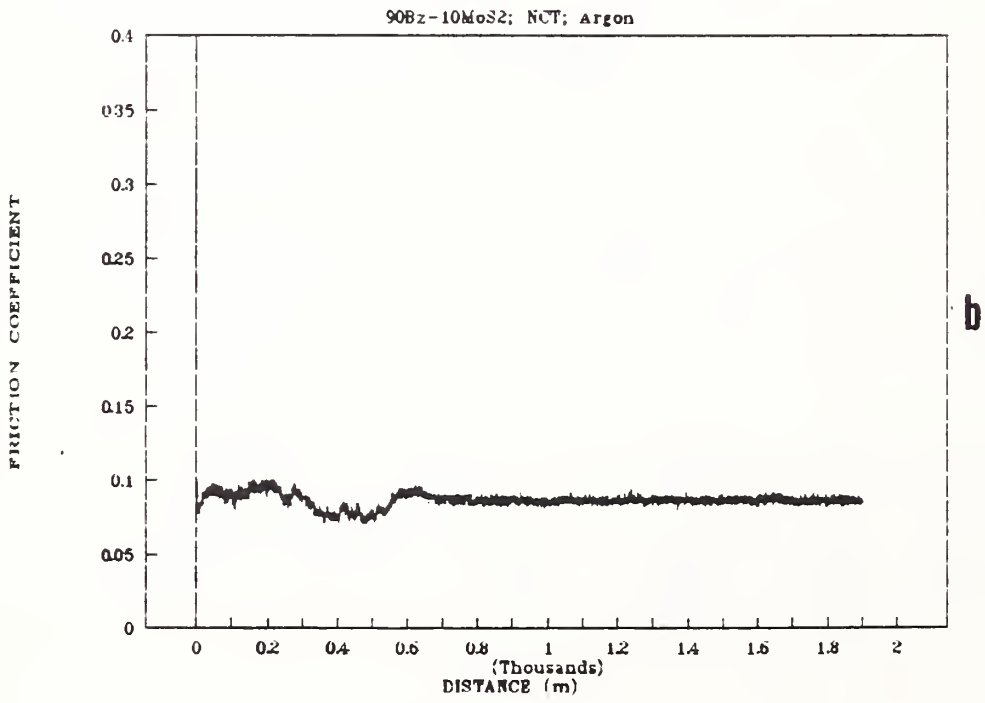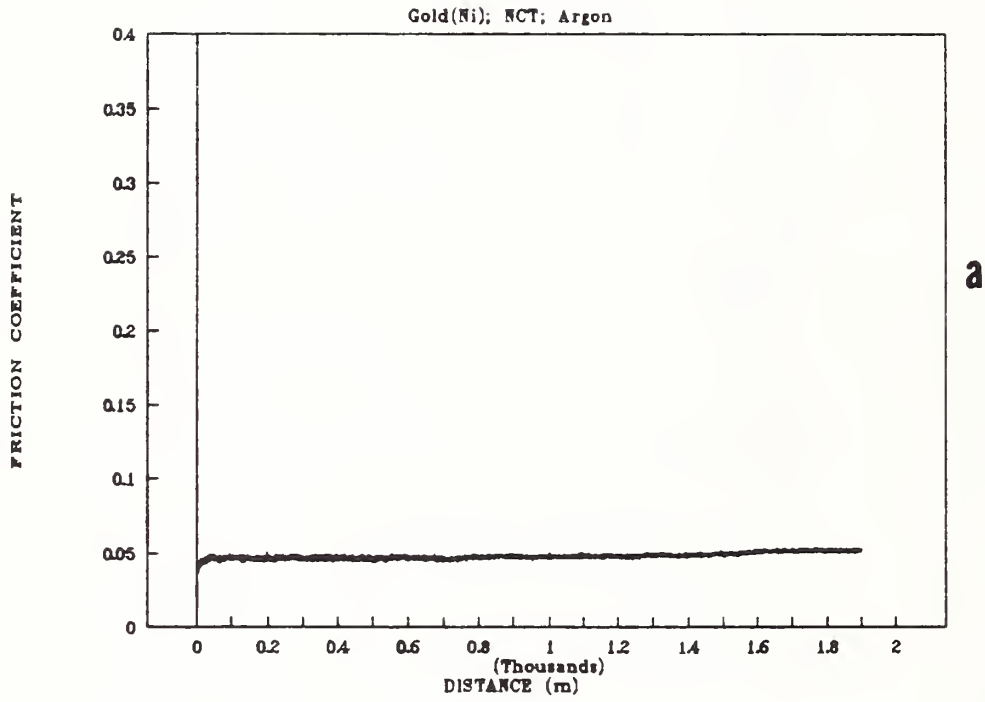
Fig. 34   Friction vs. distance results for two material combinations in argon: (a) Au vs. type MGS coating, (b) bronze-MoS$_2$ vs. type MGS coating.
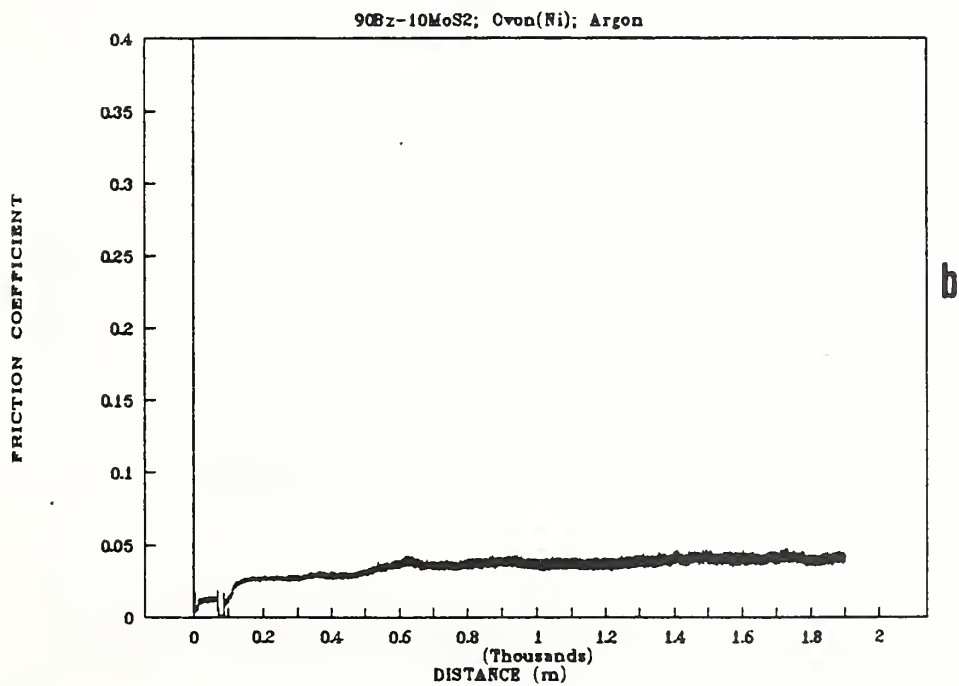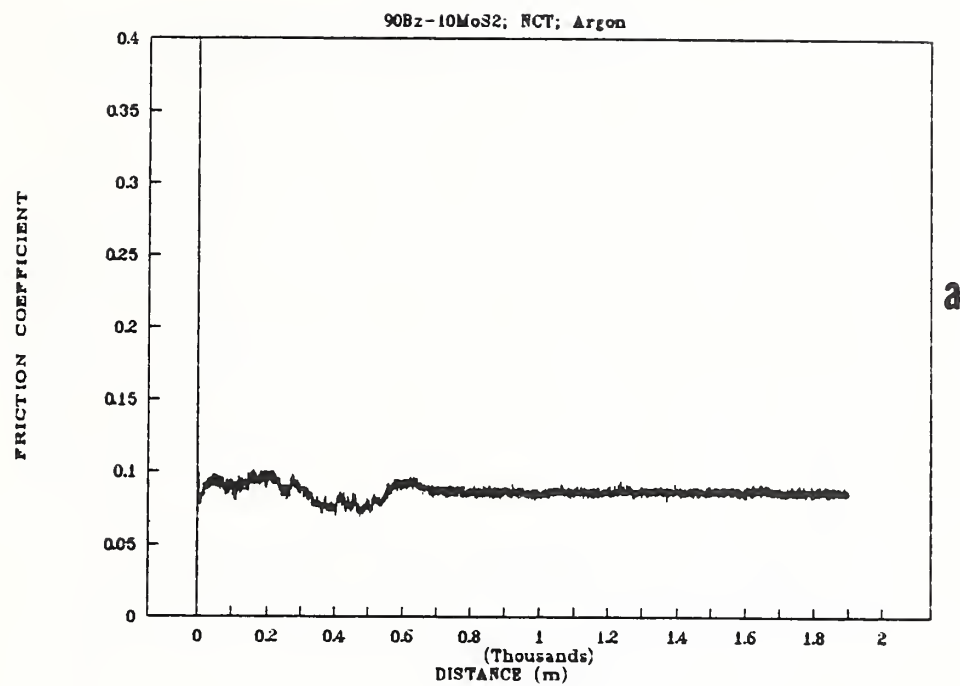
Fig. 35 Friction vs. distance results for two material combinations in argon: (a) bronze-MoS$_2$ vs. type MGS coating, (b) bronze-MoS$_2$ vs. type MLS coating.
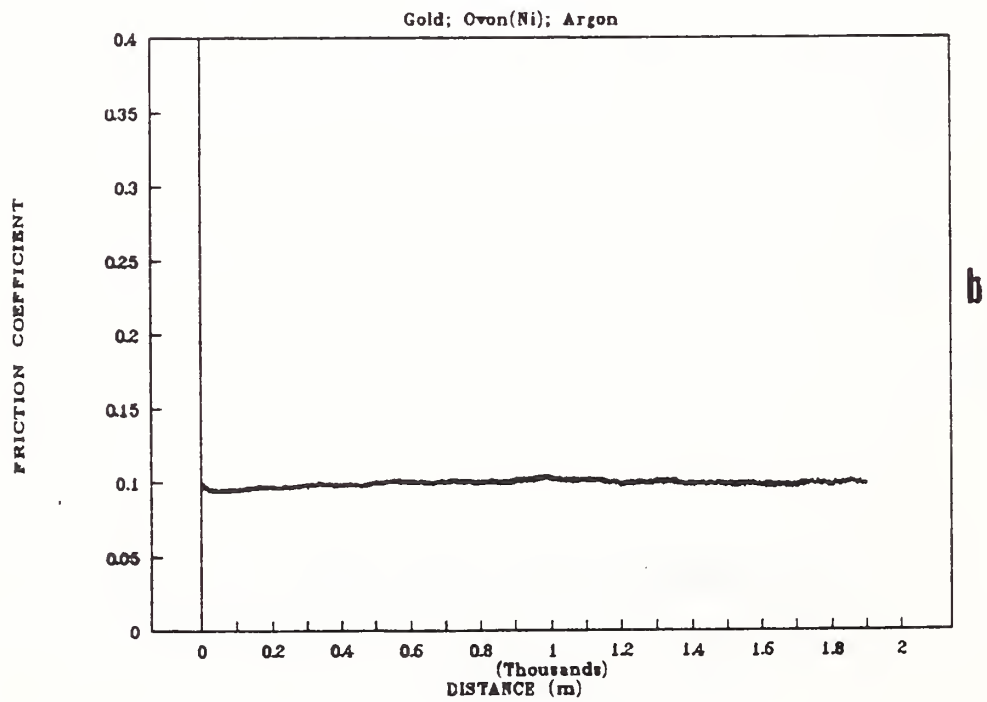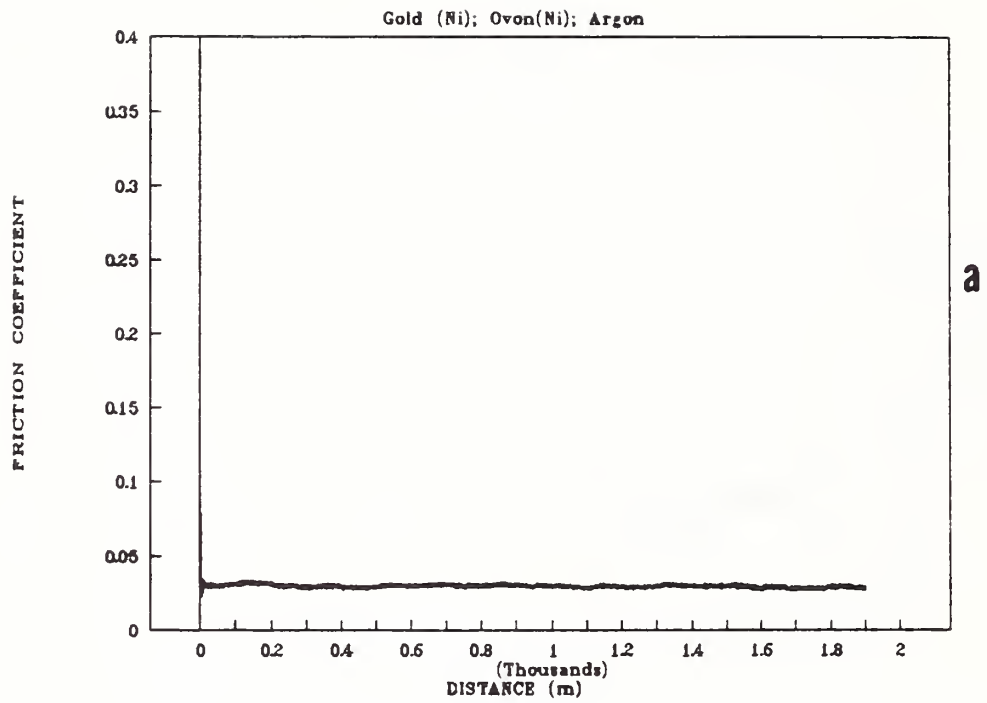
Fig. 36   Friction vs. distance results for two material combinations in
          argon: (a) Au-Ni vs. type MLS coating, (b) Au vs. type MLS coating.
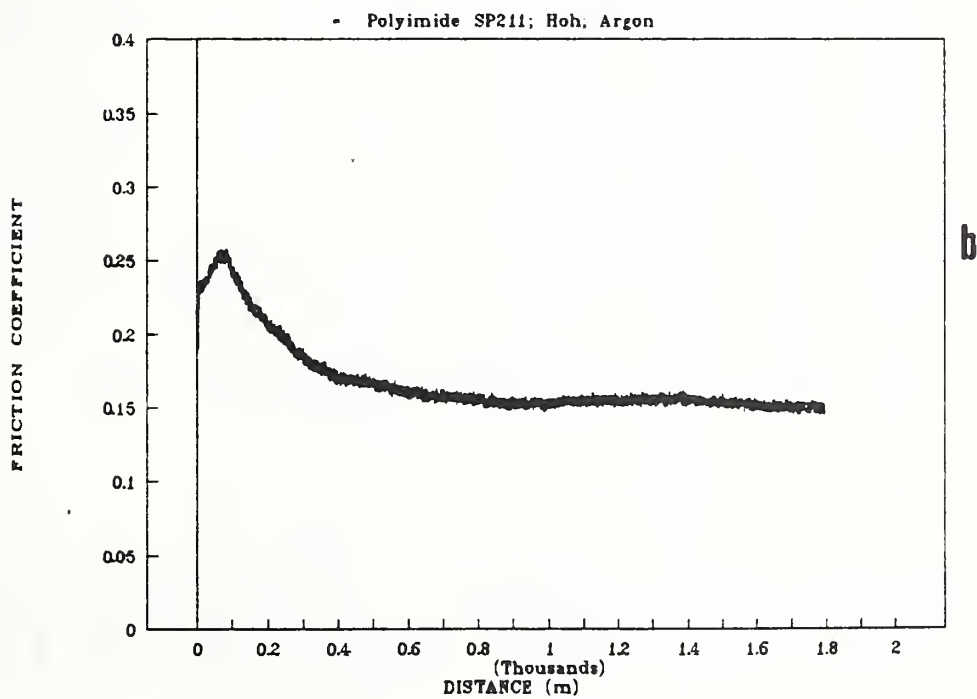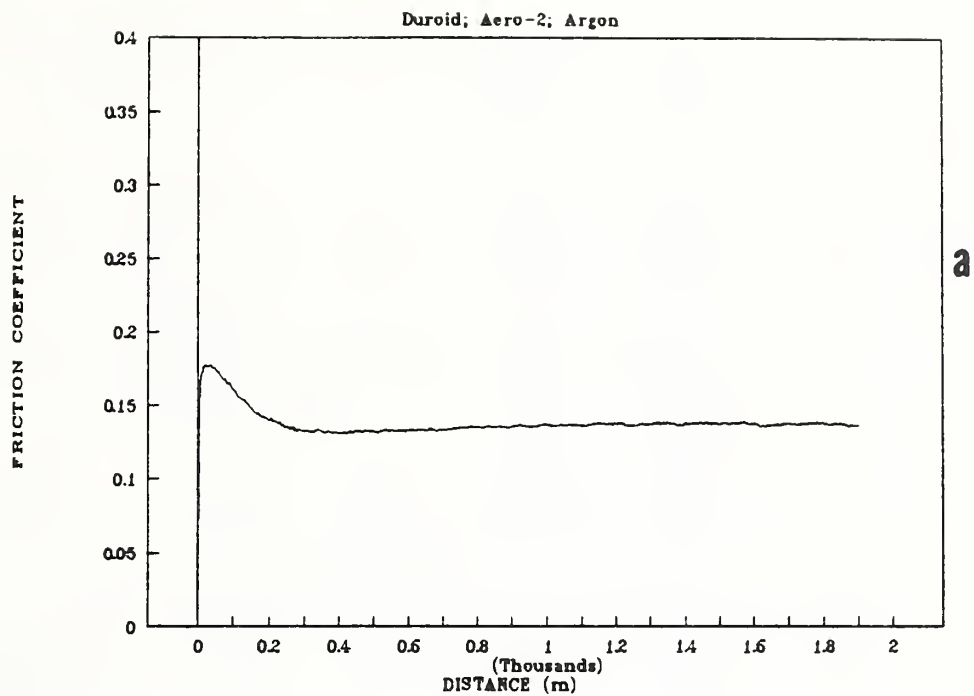
Fig. 37   Friction vs. distance results for two material combinations in argon: (a) Duroid vs. type RFS coating, (b) polyimide SP211 vs. type DCS coating.
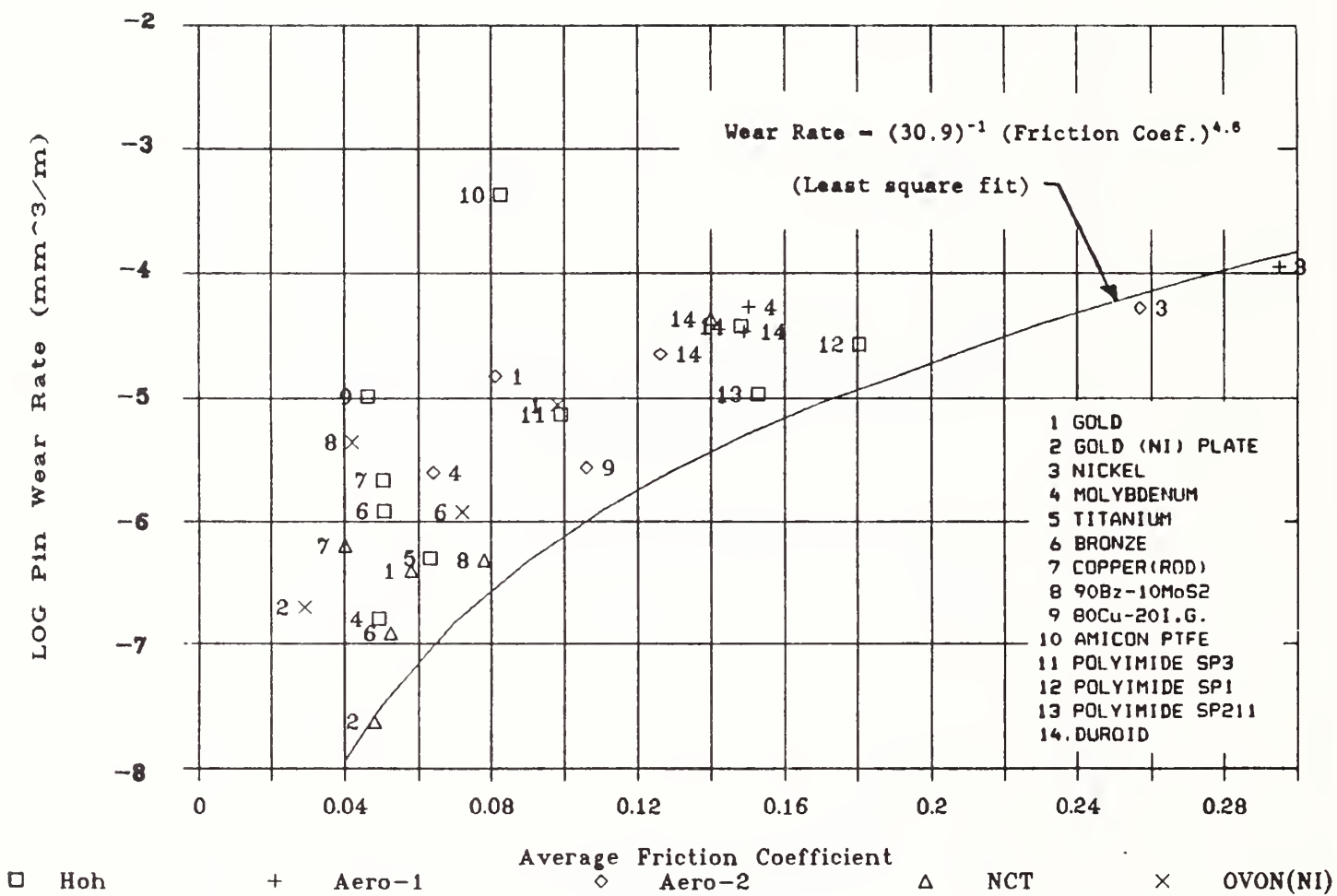
Fig. 38 Comparison of friction coefficient and wear rate results for all coatings and materials studied in dry argon atmospheres. Coating types are shown in the graph as: □ DCS, ◇+ RFS, △ MGS, ✕ MLS

Appendix A.

Table A1.   Summary of experimental data for $NiCl_2$-intercalated graphite
composites (6 parts).

DATE	TEST/PIN	PIN MATERIAL	RING MATERIAL	TEST ATMOSPHERE	TEMP (C)	CORRECTED RELATIVE HUMIDITY
05/31/88	1	Cu 5K LB	440C	LAB AIR	24	30
06/01/88	2	I.G. 5K LB	440C	LAB AIR	23	30
06/02/88	3	I.G. 5K LB	440C	LAB AIR	24	31
06/02/88	4	PbO 5K LB	440C	LAB AIR	24	31
06/02/88	5	WS2 5K LB	440C	LAB AIR	24	31
06/32/88	6	MoS2 5K LB	440C	LAB AIR	24	32
06/20/88	7A	Cu 5K LB	440C	LAB AIR	24	57
	7B	I.G. 5K LB	440C	LAB AIR	24	57
06/21/88	8A	Cu SOLID	440C	LAB AIR	25	55
	8B	I.G. 5K LB	440C	LAB AIR	25	55
06/22/88	9A	Cu SOLID	440C	LAB AIR	24	54
	9B	I.G. 5K LB	440C	LAB AIR	24	54
06/24/88	11A	Cu SOLID	440C	LAB AIR	24	41
	11B	I.G. 5K LB	440C	LAB AIR	24	41
07/07/88	12A	Cu SOLID	440C	LAB AIR	24	52
	12B	I.G. 5K LB	440C	LAB AIR	24	52
07/13/88	15A	Cu SOLID	440C	LAB AIR	24	53
	15B	I.G. 5K LB	440C	LAB AIR	24	53
06/23/88	10A	Ni SOLID	440C	LAB AIR	24	54
	10B	I.G. 5K LB	440C	LAB AIR	24	54
07/14/88	16A	Ni SOLID	440C	ARGON GAS	24	53
	16B	I.G. 5K LB	440C	ARGON GAS	24	53
07/08/88	13A	Al SOLID	440C	LAB AIR	24	55
	13B	I.G. 5K LB	440C	LAB AIR	24	55
07/12/88	14A	Al SOLID	440C	LAB AIR	24	59
	14B	I.G. 5K LB	440C	LAB AIR	24	59
08/04/88	18	I.G./Cu 20/80 10,000lb	440C	LAB AIR	24	56
08/09/88	19	Cu SOLID	440C	LAB AIR	24	52
11/07/88	20	I.G./Cu 20/80 10,000lb	440C	LAB AIR	22	30
11/08/88	21	I.G./Cu 20/80 10,000lb	440C	LAB AIR	24	31
11/08/88	22	I.G./Cu 20/80 10,000lb	440C	LAB AIR	24	31
11/10/88	23	I.G./Cu 20/80 10,000lb	440C	LAB AIR	23	40
11/10/88	24	I.G./Cu 30/70 10,000lb	440C	LAB AIR	23	40
11/10/88	25	I.G./Cu 10/90 10,000lb	440C	LAB AIR	24	40
11/14/88	26	Cu W/ LG.HOLES 10,000lb	440C	LAB AIR	22	30
11/15/88	27	Cu W/ SM.HOLES 10,000lb	440C	LAB AIR	22	29
11/28/88	28	I.G 10,000lb	440C	LAB AIR	24	26
11/28/88	29	I.G 10,000lb	52100	LAB AIR	25	22
11/29/88	30	Cu W/ LG.HOLES 10,000lb	440C	LAB AIR	24	20
11/29/88	31	Cu W/ SM.HOLES 10,000lb	440C	LAB AIR	25	20
11/29/88	32	I.G./Cu 10/90 10,000lb	440C	LAB AIR	25	20
11/29/88	33	I.G./Cu 30/70 10,000lb	440C	LAB AIR	23	20
12/01/88	34	Cu W/ .43 SLIT 10,000lb	440C	LAB AIR	23	15
12/05/88	35	Cu W/ .16 SLIT 5,000lb	440C	LAB AIR	22	9
12/06/88	36	I.G./Cu 10/90 10,000lb	440C	LAB AIR	23	11
12/07/88	37	I.G./Cu 30/70 10,000lb	440C	LAB AIR	24	13
12/07/88	38	Cu W/ LG.HOLES 10,000lb	440C	LAB AIR	24	15
12/07/88	39	Cu W/ SM.HOLES 10,000lb	440C	LAB AIR	24	15

55

Table A1 (continued).   Summary of experimental data for NiCl$_2$-intercalated graphite composites (6 parts).

DATE	TEST/PIN	LOAD (N)	DISTANCE (m)	WEAR VOLUME (mm^3)	WEAR RATE (mm^3/m)
05/31/88	1	33.11	110	0.10	9.25E-04
06/01/88	2	33.11	110	57.67	5.24E-01
06/02/88	3	33.11	55	4.00	7.27E-02
06/02/88	4	33.11	22	47.46	2.16E+00
06/02/88	5	33.11	55	12.81	2.33E-01
06/32/88	6	33.11	22	2.16	9.81E-02
06/20/88	7A	33.11	2589		
	7B	33.11	2589		
06/21/88	8A	33.11	828		
	8B	33.11	828		
06/22/88	9A	33.11	2161	0.25	1.16E-04
	9B	33.11	2161	0.51	2.36E-04
06/24/88	11A	33.11	1613	0.48	2.98E-04
	11B	33.11	1613	0.90	5.58E-04
07/07/88	12A	33.11	1734		
	12B	33.11	1734		
07/13/88	15A	33.11	1843	0.55	2.98E-04
	15B	33.11	1843	0.29	1.57E-04
06/23/88	10A	33.11	1196	0.50	4.18E-04
	10B	33.11	1196	0.85	7.11E-04
07/14/88	16A	33.11	1323	0.67	5.07E-04
	16B	33.11	1323	0.94	7.11E-04
07/08/88	13A	33.11	1824		
	13B	33.11	1824		
07/12/88	14A	33.11	1674	3.26	1.95E-03
	14B	33.11	1674	2.86	1.71E-03
08/04/88	18	33.11	790	0.34	4.36E-04
08/09/88	19	33.11	340	0.41	1.21E-03
11/07/88	20	33.11	340	0.29	8.54E-04
11/08/88	21	33.11	340	0.29	8.55E-04
11/08/88	22	33.11	790	0.58	7.32E-04
11/10/88	23	33.11	820	0.30	3.61E-04
11/10/88	24	33.11	796	0.28	3.48E-04
11/10/88	25	33.11	795	0.33	4.15E-04
11/14/88	26	33.11	810	0.30	3.69E-04
11/15/88	27	33.11	793	0.38	4.83E-04
11/28/88	28	33.11	790	7.42	9.39E-03
11/28/88	29	33.11	790	1.45	1.83E-03
11/29/88	30	33.11	790	0.19	2.45E-04
11/29/88	31	33.11	790	0.39	5.00E-04
11/29/88	32	33.11	790	0.48	6.08E-04
11/29/88	33	33.11	790	0.48	6.08E-04
12/01/88	34	33.11	790	0.43	5.48E-04
12/05/88	35	33.11	790	0.40	5.05E-04
12/06/88	36	33.11	790	0.44	5.56E-04
12/07/88	37	33.11	790	0.55	6.91E-04
12/07/88	38	33.11	790	0.23	2.85E-04
12/07/88	39	33.11	790	0.17	2.21E-04

Table A1 (continued). Summary of experimental data for NiCl$_2$-intercalated graphite composites (6 parts).

| DATE | TEST/PIN | ********************FRICTION********* | | | |
		INITIAL	FINAL	AVERAGE	MAX
05/31/88	1	0.198	0.586	0.449	0.626
06/01/88	2	0.119	0.198	0.206	0.230
06/02/88	3	0.119	0.171	0.216	0.263
06/02/88	4	0.296	0.230	0.319	0.428
06/02/88	5	0.184	0.125	0.149	0.178
06/32/88	6	0.086	0.092	0.122	0.158
06/20/88	7A	0.112			
	7B	0.112			
06/21/88	8A	0.138	0.494		
	8B	0.138	0.494		
06/22/88	9A	0.092	0.125		
	9B	0.092	0.125		
06/24/88	11A	0.079	0.151		
	11B	0.079	0.151		
07/07/88	12A	0.138	0.138	0.152	0.244
	12B	0.138	0.138	0.152	0.244
07/13/88	15A	0.135	0.172	0.178	0.310
	15B	0.135	0.172	0.178	0.310
06/23/88	10A	0.158	0.224		
	10B	0.158	0.224		
07/14/88	16A	0.303	0.573	0.591	0.676
	16B	0.303	0.573	0.591	0.676
07/08/88	13A	0.263	0.230	0.277	0.497
	13B	0.263	0.230	0.277	0.497
07/12/88	14A	0.485	0.189	0.212	0.303
	14B	0.485	0.189	0.212	0.303
08/04/88	18	0.110	0.135	0.116	0.180
08/09/88	19	0.391	0.691	0.700	0.756
11/07/88	20	0.154	0.184	0.182	0.194
11/08/88	21	0.129	0.164	0.164	0.169
11/08/88	22	0.119	0.119	0.120	0.134
11/10/88	23	0.109	0.149	0.148	0.164
11/10/88	24	0.159	0.154	0.146	0.154
11/10/88	25	0.179	0.164	0.152	0.194
11/14/88	26	0.179	0.119	0.115	0.498
11/15/88	27	0.209	0.269	0.295	0.483
11/28/88	28	0.070	0.100	0.097	0.119
11/28/88	29	0.075	0.109	0.116	0.144
11/29/88	30	0.189	0.283	0.279	0.493
11/29/88	31	0.055	0.134	0.177	0.357
11/29/88	32	0.203	0.203	0.192	0.208
11/29/88	33	0.124	0.169	0.166	0.174
12/01/88	34	0.238	0.124	0.112	0.124
12/05/88	35	0.223	0.337	0.270	0.561
12/06/88	36	0.169	0.194	0.180	0.199
12/07/88	37	0.164	0.164	0.170	0.184
12/07/88	38	0.253	0.139	0.156	0.377
12/07/88	39	0.253	0.138	0.241	0.471

Table A1 (continued). Summary of experimental data for $NiCl_2$-intercalated graphite composites (6 parts).

DATE	TEST/PIN	PIN MATERIAL	RING MATERIAL	TEST ATMOSPHERE	TEMP (C)	CORRECTED RELATIVE HUMIDITY
12/12/88	40	Cu W/ .16 SLIT 5,000lb	440C	LAB AIR	23	5
12/28/88	41	Cu W/ .41 SLITA 5,000lb	440C	ARGON	22	35
12/28/88	42	Cu W/ .43 SLITB 5,000lb	440C	ARGON	22	47
12/29/88	43	I.G./Cu 10/90 10,000lb	440C	ARGON	22	15
12/29/88	44	I.G. Cu 30/70 10,000lb	440C	ARGON	22	15
01/04/89	45	I.G./Cu 20/80 10,000lb	440C	ARGON	23	14
01/10/89	47	Cu SOLID	440C	ARGON	23	12
01/10/89	48	I.G./Cu 30/70 10,000lb	440C	ARGON	23	14
01/11/89	49	I.G./Cu 10/90 10,000lb	440C	ARGON	22	22
01/11/89	50	I.G./Cu 20/80 10,000lb	440C	ARGON	22	22
01/12/89	51	Cu SOLID W 30W MOTOR OIL	440C	LAB AIR-OIL	22	22
01/23/89	55	Cu W/ .37 SLITA 5,000lb	440C	ARGON	23	11
01/25/89	56	I.G./Cu 20/80 10,000lb	440C	ARGON/AIR	22	19
01/30/89	57	Cu W/ LG.HOLES 10,000lb	440C	ARGON/AIR	23	34
01/30/89	58	Cu SOLID	440C	ARGON	23	38
02/01/89	59	Cu SOLID	440C	ARGON	23	25
02/03/89	60	Cu SOLID	440C	ARGON	23	33
02/07/89	61	Cu SOLID	440C	LAB AIR	23	17
02/13/89	62	Cu W. LG.HOLES 10,000lb/BR	440C	LAB AIR	23	14
02/14/89	63	Cu W/ .18 SLIT 5,000lb	440C	LAB AIR	23	32
02/13/89	64	Cu W/ .17 SLIT 5,000lb	440C	ARGON	23	39
02/13/89	65	Cu W/ .17 SLIT 5,000lb	440C	ARGON	23	28
02/23/89	66	Cu SLIT .14 50/50 FILL/BR	440C	LAB AIR	22	22
02/23/89	67	Cu SLIT .14 50/50 FILL/BR	440C	LAB AIR	22	22
03/02/89	68	Cu SLIT .30, 3:1 Cu:IG/BR	440C	ARGON	23	12
03/02/89	69	Cu SLIT .28, 3:1 Cu:IG/BR	440C	ARGON	23	12
03/02/89	70	Cu SLIT .28, 3:1 Cu:IG/BR	440C	LAB AIR	23	12
03/03/89	71	Cu SLIT .29, 3:1 Cu:IG/BR	440C	LAB AIR	23	16
03/28/89	72A	I.G. 5,000 lb	440C	ARGON	23	48
03/28/89	72B	Cu SOLID 99.999%	440C	ARGON	23	48
03/28/89	73A	I.G. 5,000 lb	440C	ARGON	23	46
03/28/89	73B	Cu SOLID 99.999%	440C	ARGON	23	46
04/03/89	74A	I.G. 5,000 lb	440C	ARGON	23	40
04/03/89	74B	Cu SOLID 99.999%	440C	ARGON	23	40
04/03/89	75A	I.G. 5,000 lb	440C	ARGON	23	45
04/03/89	75B	Cu SOLID 99.999%	440C	ARGON	23	45
04/06/89	76A	I.G. 5,000 lb	440C	LAB AIR	23	28
04/06/89	76B	Cu SOLID 99.999%	440C	LAB AIR	23	28
04/10/89	77	Cu SOLID 99.999%	440C	ARGON/H2O	24	18
04/11/89	78	Cu SOLID 99.999%	440C	ARGON/H2O	24	13

Table A1 (continued).   Summary of experimental data for $NiCl_2$-intercalated graphite composites (6 parts).

DATE	TEST/PIN	LOAD (N)	DISTANCE (m)	WEAR VOLUME (mm^3)	WEAR RATE (mm^3/m)
12/12/88	40	33.11	790	0.16	2.06E-04
12/28/88	41	33.11	1604	0.21	1.32E-04
12/28/88	42	33.11	1602	0.20	1.26E-04
12/29/88	43	33.11	790	0.32	3.99E-04
12/29/88	44	33.11	790	0.40	5.10E-04
01/04/89	45	33.11	790	0.60	7.64E-04
01/10/89	47	33.11	340	0.07	2.05E-04
01/10/89	48	33.11	790	0.18	2.30E-04
01/11/89	49	33.11	790	0.60	7.57E-04
01/11/89	50	33.11	790	0.33	4.15E-04
01/12/89	51	33.11	340	0.17	5.13E-04
01/23/89	55	33.11	1600	0.35	2.16E-04
01/25/89	56	33.11	790	0.49	6.21E-04
01/30/89	57	33.11	790	0.17	2.19E-04
01/30/89	58	33.11	340	0.25	7.29E-04
02/01/89	59	33.11	340	0.06	1.76E-04
02/03/89	60	33.11	340	0.19	5.73E-04
02/07/89	61	33.11	340	0.36	1.05E-03
02/13/89	62	33.11	790	0.11	1.45E-04
02/14/89	63	33.11	790	0.20	2.59E-04
02/13/89	64	33.11	790	0.08	9.59E-05
02/13/89	65	33.11	790	0.06	8.21E-05
02/23/89	66	33.11	790	1.02	1.29E-03
02/23/89	67	33.11	790	0.39	4.90E-04
03/02/89	68	33.11	790	0.10	1.24E-04
03/02/89	69	33.11	790	0.16	1.99E-04
03/02/89	70	33.11	790	0.95	1.21E-03
03/03/89	71	33.11	790	0.84	1.06E-03
03/28/89	72A	33.11	790	0.45	5.69E-04
03/28/89	72B	33.11	790	0.36	4.56E-04
03/28/89	73A	33.11	790	0.36	4.56E-04
03/28/89	73B	33.11	790	0.29	3.67E-04
04/03/89	74A	33.11	790	0.30	3.80E-04
04/03/89	74B	33.11	790	0.18	2.28E-04
04/03/89	75A	33.11	790	0.11	1.39E-04
04/03/89	75B	33.11	790	0.13	1.64E-04
04/06/89	76A	33.11	790	0.08	1.04E-04
04/06/89	76B	33.11	790	0.24	3.04E-04
04/10/89	77	33.11	790	0.73	9.22E-04
04/11/89	78	33.11	790	0.61	7.70E-04

Table Al (continued).   Summary of experimental data for $NiCl_2$-intercalated graphite composites (6 parts).

| DATE | TEST/PIN | *****************FRICTION********* | | | |
		INITIAL	FINAL	AVERAGE	MAX
12/12/88	40	0.236	0.203	0.196	0.359
12/28/88	41	0.097	0.223	0.190	0.237
12/28/88	42	0.320	0.339	0.322	0.368
12/29/88	43	0.271	0.228	0.230	0.257
12/29/88	44	0.150	0.087	0.084	0.087
01/04/89	45	0.160	0.126	0.114	0.131
01/10/89	47	0.284	0.468	0.411	0.468
01/10/89	48	0.139	0.119	0.116	0.119
01/11/89	49	0.147	0.216	0.191	0.216
01/11/89	50	0.116	0.068	0.064	0.068
01/12/89	51	0.258	0.113	0.123	0.145
01/23/89	55	0.210	0.233	0.199	0.252
01/25/89	56				
01/30/89	57				
01/30/89	58	0.265	0.462	0.435	0.500
02/01/89	59	0.251	0.464	0.415	0.513
02/03/89	60	0.249	0.439	0.482	0.559
02/07/89	61	0.309	0.440	0.462	0.687
02/13/89	62	0.158	0.215	0.198	0.232
02/14/89	63	0.264	0.275	0.259	0.429
02/13/89	64	0.159	0.332	0.309	0.369
02/13/89	65	0.146	0.269	0.283	0.353
02/23/89	66	0.126	0.587	0.562	0.691
02/23/89	67	0.161	0.529	0.467	0.763
03/02/89	68	0.136	0.444	0.336	0.475
03/02/89	69	0.155	0.403	0.375	0.655
03/02/89	70	0.131	0.622	0.525	0.700
03/03/89	71	0.185	0.590	0.544	0.715
03/28/89	72A	0.171	0.279	0.272	0.338
03/28/89	72B	0.171	0.279	0.272	0.338
03/28/89	73A	0.200	0.230	0.240	0.302
03/28/89	73B	0.200	0.230	0.240	0.302
04/03/89	74A	0.108	0.219	0.203	0.250
04/03/89	74B	0.108	0.219	0.203	0.250
04/03/89	75A	0.291	0.240	0.235	0.298
04/03/89	75B	0.291	0.240	0.235	0.298
04/06/89	76A	0.228	0.232	0.218	0.343
04/06/89	76B	0.228	0.232	0.218	0.343
04/10/89	77	0.262	0.570	0.534	0.729
04/11/89	78	0.314	0.560	0.545	0.645

Table A2.   Summary of experimental data for MoS$_2$ composites (3 parts).

DATE	TEST/PIN PIN MATERIAL	RING MATERIAL	TEST ATMOSPHERE	TEMP (C)	CORRECTED RELATIVE HUMIDITY
12-27-89	117 MoS2/Cu 30/70 5,000 lb	440C	ARGON	23	15
01-02-90	118 MoS2/Cu 30/70 5,000 lb	440C	LAB AIR	23	17
01-02-90	119 MoS2/Cu 20/80 5,000 lb	440C	ARGON	23	17
01-03-90	120 MoS2/Cu 20/80 5,000 lb	440C	LAB AIR	24	19
01-08-90	121 MoS2/Cu 10/90 5,000 lb	440C	LAB AIR	23	21
01-09-90	122 MoS2/Cu 10/90 5,000 lb	440C	ARGON	23	24
01-10-90	123 Cu 100% 5,000 lb	440C	LAB AIR	23	26
01-17-90	124 Cu 100% 5,000 lb	440C	ARGON	23	29
01-17-90	125 MoS2/Cu SM. HOLES 10,000 lb	440C	LAB AIR	23	33
01-22-90	126 MoS2/Cu LG. HOLES 10,000 lb	440C	ARGON	24	21
01-22-90	127 MoS2/Cu 10/90 5,000 lb	440C	LAB AIR	24	21
01-23-90	128 MoS2/Cu 10/90 5,000 lb	440C	ARGON	24	21
01-24-90	129 MoS2/Cu 20/80 5,000 lb	440C	LAB AIR	24	27
01-24-90	130 MoS2/Cu 20/80 5,000 lb	440C	ARGON	23	27
01-29-90	131 MoS2/Cu 30/70 5,000 lb	440C	LAB AIR	24	20
01-29-90	132 MoS2/Cu 30/70 5,000 lb	440C	ARGON	24	24
01-30-90	133 Cu 100% 5,000 lb	440C	LAB AIR	24	23
01-30-90	134 MoS2/Cu SM. HOLES 10,000 lb	440C	LAB AIR	24	23
01-31-90	135 MoS2/Cu LG. HOLES 10,000 lb	440C	ARGON	24	23
02-07-90	136 MoS2/Cu SM. HOLES 10,000 lb	440C	ARGON	24	28
02-07-90	137 MoS2/Cu LG. HOLES 10,000 lb	440C	LAB AIR	24	30
05-08-90	138 MoS2/BZ 8/92 5,000 lb	52100	ARGON	24	38
05-08-90	139 MoS2/BZ 8/92 5,000 lb	52100	LAB AIR	24	38
05-09-90	140 BZ 20um W/MoS2 COMPRESSED 5K#	52100	LAB AIR	24	47
05-09-90	141 BZ 20um W/MoS2 COMPRESSED 5K#	440C	ARGON	24	47
05-11-90	142 BZ 20um W/MoS2 COMPRESSED 5K#/BRN	440C	ARGON	24	33
05-11-90	143 BZ PRESSED 5K#	440C	ARGON	24	33
05-14-90	144 2PIN: BZ 15um COMPR 5K#+MoS2 5K#	440C	ARGON	24	43
05-15-90	145 2PIN: ANLD BZ 15um COMPR 5K#+MoS2 5K#	440C	ARGON	24	52
05-15-90	146 BZ 20um W/MoS2 COMPR. 5K#/BRN/ANLD	440C	ARGON	24	54
05-16-90	147 BZ 15um COMPRESSED 5K#/ANLD	440C	ARGON	23	59

Table A2 (continued).   Summary of experimental data for MoS$_2$ composites (3 parts).

DATE	TEST/PIN	LOAD (N)	DISTANCE (m)	WEAR SCAR SIZE1(AVG) (mm)	WEAR SCAR SIZE2(AVG) (mm)	MoS2 WEAR VOL 2P(mm^3)	CALC. WEAR VOL (mm^3)	WEAR RATE (mm^3/m)
12-27-89	117	33.11	812	2.325			3.81E-01	4.69E-04
01-02-90	118	33.11	800	4.328			2.38E+00	2.98E-03
01-02-90	119	33.11	801	2.931			7.62E-01	9.51E-04
01-03-90	120	33.11	791	5.454			4.63E+00	5.85E-03
01-08-90	121	33.11	790	6.104			6.33E+00	8.01E-03
01-09-90	122	33.11	794	5.821			5.55E+00	7.00E-03
01-10-90	123	33.11	793	1.895			2.06E-01	2.60E-04
01-17-90	124	33.11	794	1.572			1.18E-01	1.49E-04
01-17-90	125	33.11	792	2.670			5.87E-01	7.41E-04
01-22-90	126	33.11	791	2.051			2.61E-01	3.30E-04
01-22-90	127	33.11	791	5.950			5.94E+00	7.51E-03
01-23-90	128	33.11	795	5.308			4.31E+00	5.42E-03
01-24-90	129	33.11	792	5.509			4.76E+00	6.02E-03
01-24-90	130	33.11	792	3.370			1.14E+00	1.44E-03
01-29-90	131	33.11	794	3.952			1.83E+00	2.30E-03
01-29-90	132	33.11	792	2.433			4.39E-01	5.54E-04
01-30-90	133	33.11	794	3.270			1.05E+00	1.32E-03
01-30-90	134	33.11	793	1.885			2.03E-01	2.57E-04
01-31-90	135	33.11	796	1.974			2.34E-01	2.94E-04
02-07-90	136	33.11	792	1.400			8.33E-02	1.05E-04
02-07-90	137	33.11	793	4.342			2.41E+00	3.03E-03
05-08-90	138	33.11	794	5.862			5.67E+00	7.14E-03
05-08-90	139	33.11	793	4.731			3.07E+00	3.87E-03
05-09-90	140	33.11	791	2.734			6.15E-01	7.77E-04
05-09-90	141	33.11	790	1.767			1.67E-01	2.12E-04
05-11-90	142	33.11	791	1.929			2.18E-01	2.75E-04
05-11-90	143	33.11	794	1.800			1.80E-01	2.26E-04
05-14-90	144	33.11	794	1.043	0.730	5.00E-02	1.10E-01	1.39E-04
05-15-90	145	33.11	790	1.330	0.887	9.00E-02	2.20E-01	2.78E-04
05-15-90	146	33.11	791	1.657			1.38E-01	1.75E-04
05-16-90	147	33.11	790	1.956			2.27E-01	2.87E-04

Table A2 (continued). Summary of experimental data for MoS$_2$ composites (3 parts).

DATE	TEST/PIN	************************FRICTION**********			
		INITIAL	FINAL	AVERAGE	MAX
12-27-89	117	0.161	0.102	0.103	0.109
01-02-90	118	0.174	0.148	0.153	0.171
01-02-90	119	0.217	0.065	0.070	0.788
01-03-90	120	0.177	0.141	0.152	0.200
01-08-90	121	0.207	0.009	0.054	0.118
01-09-90	122	0.185	0.056	0.063	0.075
01-10-90	123	0.259	0.674	0.645	0.764
01-17-90	124	0.227	0.468	0.448	0.600
01-17-90	125	0.195	0.237	0.120	0.451
01-22-90	126	0.142	0.104	0.208	0.364
01-22-90	127	0.168	0.061	0.096	0.145
01-23-90	128	0.191	0.080	0.086	0.098
01-24-90	129	0.160	0.130	0.159	0.200
01-24-90	130	0.220	0.075	0.081	0.095
01-29-90	131	0.171	0.152	0.145	0.171
01-29-90	132	0.132	0.069	0.070	0.075
01-30-90	133	0.280	0.511	0.530	0.666
01-30-90	134	0.147	0.146	0.167	0.445
01-31-90	135	0.263	0.134	0.193	0.427
02-07-90	136	0.193	0.441	0.451	0.639
02-07-90	137	0.234	0.124	0.144	0.572
05-08-90	138	0.075	0.060	0.067	0.126
05-08-90	139	0.245	0.099	0.119	0.183
05-09-90	140	0.221	0.543	0.533	0.623
05-09-90	141	0.202	0.422	0.399	0.510
05-11-90	142	0.156	0.394	0.396	0.496
05-11-90	143	0.217	0.515	0.470	0.601
05-14-90	144	0.168	0.104	0.132	0.253
05-15-90	145	0.194	0.145	0.298	0.461
05-15-90	146	0.204	0.360	0.360	0.431
05-16-90	147	0.183	0.442	0.461	0.588

Table A3. Summary of experimental data for MoS$_2$-coated 440C steel rings (3 parts).

DATE	TEST/PIN	PIN MATERIAL	RING MATERIAL (STEEL)	TEST ATMOSPHERE	TEMP (C)	CORRECTED RELATIVE HUMIDITY
06/28/89	81	BRONZE, 1/8in	440C,Hohman MoS2	ARGON	24	61
06/29/89	82	BRONZE, 1/8in	440C,Hohman MoS2	LAB AIR	23	55
06/29/89	83	AMICON PTFE,1/8in	440C,Hohman MoS2	LAB AIR	23	55
06/30/89	84	AMICON PTFE,1/8in	440C,Hohman MoS2	ARGON	23	44
07/03/89	85	TITANIUM,1/8in	440C,Hohman MoS2	ARGON/AIR	23	60
07/05/89	86	TITANIUM,1/8in	440C,Hohman MoS2	ARGON	23	61
07/06/89	87	POLYIMIDE SP3,1/8in	440C,Hohman MoS2	ARGON	23	61
07/10/89	88	POLYIMIDE SP3,1/8in	440C,Hohman MoS2	LAB AIR	23	61
07/11/89	89	MOLYBDENUM,1/8in	440C,Hohman MoS2	ARGON	23	62
07/12/89	90	MOLYBDENUM,1/8in	440C,Hohman MoS2	LAB AIR	23	61
07/17/89	91	POLYIMIDE SP1,1/8in	440C,Hohman MoS2	ARGON	23	61
07/18/89	92	POLYIMIDE SP1,1/8in	440C,Hohman MoS2	LAB AIR	23	61
07/19/89	93	POLYIMIDE SP211.1/8in	440C,Hohman MoS2	ARGON	23	61
07/20/89	94	POLYIMIDE SP211,1/8in	440C,Hohman MoS2	LAB AIR	23	63
07/24/89	95	DUROID,1.6mm	440C,Hohman MoS2	ARGON	23	63
07/25/89	96	DUROID,1.6mm	440C,Hohman MoS2	LAB AIR	23	63
07/26/89	97	COPPER (FROM ROD),1/8in	440C,Hohman MoS2	ARGON	23	61
07/27/89	98	COPPER (FROM ROD),1/8in	440C,Hohman MoS2	LAB AIR	23	63
07/31/89	99	Cu-I.G. 80/20,1.6mm	440C,Hohman MoS2	ARGON	23	60
08/01/89	100	Cu-I.G. 80/20,1.6mm	440C,Hohman MoS2	LAB AIR	23	62
11/07/89	101	DUROID,1.6mm	440C,Aerosp. MoS2/R1	ARGON	23	39
11/08/89	102	DUROID,1.6mm	440C,Aerosp. MoS2/R1	LAB AIR	23	44
11/09/89	103	NICKEL,1/8in	440C,Aerosp. MoS2/R1	ARGON	23	58
11/13/89	104	NICKEL,1/8in	440C,Aerosp. MoS2/R1	LAB AIR	23	21
11/14/89	105	MOLYBDENUM,1/8in	440C,Aerosp. MoS2/R1	ARGON	23	55
11/15/89	106	MOLYBDENUM,1/8in	440C,Aerosp. MoS2/R1	LAB AIR	23	55
11/20/89	107	Cu-I.G. 80/20,1.86mm	440C,Aerosp. MoS2/R2	LAB AIR	23	21
11/21/89	108	Cu-I.G. 80/20,1.86mm	440C,Aerosp. MoS2/R2	ARGON	23	17
11/22/89	109	MOLYBDENUM,1/8in	440C,Aerosp. MoS2/R2	LAB AIR	23	17
11/27/89	110	MOLYBDENUM,1/8in	440C,Aerosp. MoS2/R2	ARGON	23	24
11/28/89	111	DUROID,1.6mm	440C,Aerosp. MoS2/R2	ARGON	23	41
11/29/89	112	DUROID,1.6mm	440C,Aerosp. MoS2/R2	LAB AIR	23	20
12/04/89	113	NICKEL,1/8in	440C,Aerosp. MoS2/R2	LAB AIR	23	18
12/05/89	114	NICKEL,1/8in	440C,Aerosp. MoS2/R2	ARGON	23	17
12/06/89	115	GOLD,1/8in	440C,Aerosp. MoS2/R2	ARGON	23	20
12/11/89	116	GOLD,1/8in	440C,Aerosp. MoS2/R2	LAB AIR	23	20
06/06/90	148	GOLD,1/8in,1/4" radius	440C,NCT MoS2	ARGON	23	47
06/07/90	149	BRONZE,1/8in,1/4" radius	440C,NCT MoS2	ARGON	29	59
06/11/90	150	BRONZE,1/8in,flat end	440C,NCT MoS2	ARGON	24	46
06/12/90	151	Au/Ni PLT STEEL,1/8in,1/4"r	440C,NCT MoS2	ARGON	24	43
06/13/90	152	Cu,1/8in,1/4" radius	440C,NCT MoS2	ARGON	23	49
06/14/90	153	DUROID FLAT END STRIP	440C,NCT MoS2	ARGON	23	56
06/19/90	154	Au/Ni PLT STEEL,1/8in,1/4"r	440C,NCT MoS2	ARGON	23	61
06/20/90	155	BZ 20um W/MoS2,CPR@5K#,ANL	440C,NCT MoS2	ARGON	23	51
06/21/90	156	BZ 100um W/MoS2 CPR@5K#	440C,NCT MoS2	ARGON	23	58
06/25/90	157	BZ 20um W/MoS2,CPR@5K#,ANL	440C,NCT MoS2	ARGON	23	49
01/24/91	158	BZ 20um W/MoS2,CPR@5K#,ANL	440C,Ovonics MoS2	ARGON	24	25
01/25/91	159	Au/Ni PLT STEEL,1/8in,1/4"r	440C,Ovonics MoS2	ARGON	23	23
01/28/91	160	BRONZE,1/8in,flat end	440C,Ovonics MoS2	ARGON	23	27
01/29/91	161	GOLD,1/8in	440C,Ovonics MoS2	ARGON	24	28

64

DATE	TEST/PIN	LOAD (N)	DISTANCE (m)	WEAR SCAR SIZE1 (AVG) (mm)	WEAR SCAR SIZE2 (AVG) (mm)	CALC. WEAR VOL (mm^3)	WEAR RATE (mm^3/m)
06/28/89	81	33.11	1900	0.737		2.34E-03	1.23E-06
06/29/89	82	33.11	200	2.560		3.47E-01	1.73E-03
06/29/89	83	33.11	1900	2.590		3.64E-01	1.91E-04
06/30/89	84	33.11	1900	3.170		8.18E-01	4.31E-04
07/03/89	85	33.11	1900	0.672			
07/05/89	86	33.11	1900	0.589		9.53E-04	5.02E-07
07/06/89	87	33.11	1900	1.150		1.40E-02	7.36E-06
07/10/89	88	33.11	1900	1.780		8.07E-02	4.25E-05
07/11/89	89	33.11	1900	0.445		3.09E-04	1.63E-07
07/12/89	90	33.11	476	1.050		9.70E-03	2.04E-05
07/17/89	91	33.11	1900	1.590		5.13E-02	2.70E-05
07/18/89	92	33.11	1900	1.800		8.44E-02	4.44E-05
07/19/89	93	33.11	1900	1.260		2.02E-02	1.06E-05
07/20/89	94	33.11	1900	1.170		1.50E-02	7.88E-06
07/24/89	95	33.11	1900	2.500	1.6	7.20E-02	3.79E-05
07/25/89	96	33.11	1900	1.800	1.6	2.70E-02	1.42E-05
07/26/89	97	33.11	1900	0.848		4.12E-03	2.17E-06
07/27/89	98	33.11	304	1.260		2.02E-02	6.63E-05
07/31/89	99	33.11	1900	1.720	1.6	1.95E-02	1.03E-05
08/01/89	100	33.11	1900	3.000	1.6	6.50E-02	3.42E-05
11/07/89	101	33.11	1900	2.420	1.6	6.54E-02	3.44E-05
11/08/89	102	33.11	1900	2.100	1.6	4.27E-02	2.25E-05
11/09/89	103	33.11	1900	2.275		2.16E-01	1.14E-04
11/13/89	104	33.11	1208	2.442		2.87E-01	2.38E-04
11/14/89	105	33.11	1900	1.888		1.02E-01	5.38E-05
11/15/89	106	33.11	1134	1.071		1.05E-02	9.26E-06
11/20/89	107	33.11	1900	2.300	1.86	1.09E-01	5.74E-05
11/21/89	108	33.11	1900	1.000	1.09	5.19E-03	2.73E-06
11/22/89	109	33.11	1274	2.240		2.03E-01	1.59E-04
11/27/89	110	33.11	1900	0.880		4.77E-03	2.51E-06
11/28/89	111	33.11	1900	2.100	1.6	4.27E-02	2.25E-05
11/29/89	112	33.11	1900	1.800	1.6	2.70E-02	1.42E-05
12/04/89	113	33.11	1900	2.970		6.30E-01	3.31E-04
12/05/89	114	33.11	1900	1.880		1.00E-01	5.29E-05
12/06/89	115	33.11	1900	1.370		2.82E-02	1.49E-05
12/11/89	116	33.11	1900	1.520		4.28E-02	2.25E-05
06/06/90	148	33.11	1509			6.10E-04	3.21E-07
06/07/90	149	33.11	1901			3.50E-04	1.84E-07
06/11/90	150	33.11	1901			1.30E-04	6.84E-08
06/12/90	151	33.11	1904			3.50E-05	1.84E-08
06/13/90	152	33.11	1903			1.20E-03	6.32E-07
06/14/90	153	33.11	1900			8.20E-02	4.32E-05
06/19/90	154	33.11	1901			5.50E-05	2.89E-08
06/20/90	155	33.11	1901			8.40E-04	4.42E-07
06/21/90	156	33.11	1901			7.20E-03	3.79E-06
06/25/90	157	33.11	1903			1.00E-03	5.30E-07
01/24/91	158	33.11	1900			8.40E-03	4.40E-06
01/25/91	159	33.11	1900			3.80E-04	2.00E-07
01/28/91	160	33.11	1900			1.20E-03	1.20E-06
01/29/91	161	33.11	1900			1.70E-02	8.80E-06

Table A3 (continued).   Summary of experimental data for MoS$_2$-coated 440C
steel rings (3 parts).

| DATE | TEST/PIN | *******************FRICTION********* | | | |
		INITIAL	FINAL	AVERAGE	MAX
06/28/89	81	0.060	0.052	0.051	0.100
06/29/89	82	0.086	0.229	0.170	0.229
06/29/89	83	0.162	0.157	0.166	0.179
06/30/89	84	0.156	0.059	0.083	0.169
07/03/89	85	0.076	0.200	0.200	0.240
07/05/89	86	0.083	0.060	0.063	0.133
07/06/89	87	0.320	0.086	0.099	0.339
07/10/89	88	0.228	0.289	0.292	0.337
07/11/89	89	0.050	0.048	0.049	0.065
07/12/89	90	0.071	0.374	0.438	0.502
07/17/89	91	0.275	0.130	0.180	0.317
07/18/89	92	0.235	0.257	0.274	0.293
07/19/89	93	0.228	0.128	0.153	0.254
07/20/89	94	0.190	0.252	0.267	0.297
07/24/89	95	0.156	0.118	0.148	0.162
07/25/89	96	0.145	0.142	0.150	0.157
07/26/89	97	0.054	0.049	0.050	0.085
07/27/89	98	0.166	0.457	0.416	0.522
07/31/89	99	0.039	0.046	0.046	0.052
08/01/89	100	0.357	0.123	0.143	0.506
11/07/89	101	0.165	0.144	0.149	0.197
11/08/89	102	0.151	0.143	0.149	0.160
11/09/89	103	0.106	0.340	0.295	0.567
11/13/89	104	0.187	0.301	0.359	0.518
11/14/89	105	0.113	0.073	0.150	0.495
11/15/89	106	0.132	0.478	0.485	0.570
11/20/89	107	0.186	0.236	0.223	0.272
11/21/89	108	0.110	0.105	0.106	0.114
11/22/89	109	0.063	0.103	0.224	0.568
11/27/89	110	0.051	0.061	0.064	0.132
11/28/89	111	0.144	0.112	0.126	0.156
11/29/89	112	0.164	0.137	0.138	0.178
12/04/89	113	0.150	0.300	0.386	0.615
12/05/89	114	0.100	0.458	0.257	0.520
12/06/89	115	0.101	0.082	0.081	0.121
12/11/89	116	0.095	0.168	0.122	0.182
06/06/90	148		0.059	0.058	0.061
06/07/90	149	0.035	0.049	0.049	0.051
06/11/90	150	0.081	0.056	0.056	0.061
06/12/90	151	0.055	0.049	0.048	0.051
06/13/90	152	0.092	0.039	0.038	0.042
06/14/90	153	0.134	0.100	0.146	0.185
06/19/90	154	0.061	0.052	0.048	0.054
06/20/90	155	0.043	0.086	0.086	0.100
06/21/90	156	0.067	0.083	0.083	0.089
06/25/90	157	0.049	0.070	0.070	0.074
01/24/91	158	0.011	0.042	0.042	0.045
01/25/91	159	0.030	0.029	0.029	0.032
01/28/91	160	0.045	0.072	0.072	0.078
01/29/91	161	0.080	0.098	0.098	0.104

4. TITLE AND SUBTITLE

Tribological Investigations of Composites and Other Selected Materials Sliding Against Vacuum-Deposited MoS_2 Coatings

5. AUTHOR(S)

A. W. Ruff and M. B. Peterson

6. PERFORMING ORGANIZATION (IF JOINT OR OTHER THAN NIST, SEE INSTRUCTIONS)

U.S. DEPARTMENT OF COMMERCE
NATIONAL INSTITUTE OF STANDARDS AND TECHNOLOGY
GAITHERSBURG, MD 20899

7. CONTRACT/GRANT NUMBER

FY1457-91N-5026

8. TYPE OF REPORT AND PERIOD COVERED

FINAL - FY 89-92

9. SPONSORING ORGANIZATION NAME AND COMPLETE ADDRESS (STREET, CITY, STATE, ZIP)

Air Force Materials Lab
ATTN: K. Mecklenburg - MLBT
Wright Patterson AFB, OH 45433-6533

10. SUPPLEMENTARY NOTES

11. ABSTRACT (A 200-WORD OR LESS FACTUAL SUMMARY OF MOST SIGNIFICANT INFORMATION. IF DOCUMENT INCLUDES A SIGNIFICANT BIBLIOGRAPHY OR LITERATURE SURVEY, MENTION IT HERE.)

A new materials approach for rolling element bearings in space satellite systems involves the use of solid lubricating retainers and pre-MoS_2 vacuum coated bearing elements. Improved vacuum deposition methods are now available to produce dense, suitably oriented, durable films of molybdenum disulfide. It is of interest to examine materials in sliding contact with such films in order to identify suitable combinations, and to further improve tribological performance of the system. Results of wear and friction measurements are presented on a number of materials including self-lubricating composites sliding against four different types of vacuum-deposited MoS_2 films. The testing program utilized a controlled environment, pin-on-ring tribometer, with load and speed conditions appropriate to a possible application. Differences in wear over 4 orders of magnitude, and friction up to a factor of 7, were measured among the materials. Several promising material combinations are identified.

12. KEY WORDS (6 TO 12 ENTRIES; ALPHABETICAL ORDER; CAPITALIZE ONLY PROPER NAMES; AND SEPARATE KEY WORDS BY SEMICOLONS)

bearing; coating; friction; materials; molybdenum disulfide; retainer; solid lubricant; tribology; wear

13. AVAILABILITY

[X] UNLIMITED

[ ] FOR OFFICIAL DISTRIBUTION. DO NOT RELEASE TO NATIONAL TECHNICAL INFORMATION SERVICE (NTIS).

[ ] ORDER FROM SUPERINTENDENT OF DOCUMENTS, U.S. GOVERNMENT PRINTING OFFICE, WASHINGTON, DC 20402.

[X] ORDER FROM NATIONAL TECHNICAL INFORMATION SERVICE (NTIS), SPRINGFIELD, VA 22161.

14. NUMBER OF PRINTED PAGES

73

15. PRICE

A04

ELECTRONIC FORM